A COMPARISON OF SPATIAL MODULATION AND SPATIAL MULTIPLEXING SYSTEMS IN MULTIPATH FADING CHANNELS

A THESIS SUBMITTED TO
THE GRADUATE SCHOOL OF NATURAL AND APPLIED SCIENCES
OF
MIDDLE EAST TECHNICAL UNIVERSITY

BY

HALİL SAYGILI

IN PARTIAL FULFILLMENT OF THE REQUIREMENTS
FOR
THE DEGREE OF MASTER OF SCIENCE
IN
ELECTRICAL AND ELECTRONICS ENGINEERING

SEPTEMBER 2013

Approval of the thesis:

A COMPARISON OF SPATIAL MODULATION AND SPATIAL MULTIPLEXING SYSTEMS IN MULTIPATH FADING CHANNELS

submitted by **HALİL SAYGILI** in partial fulfillment of the requirements for the degree of **Master of Science in Electrical and Electronics Engineering Department, Middle East Technical University** by,

Prof. Dr. Canan Özgen _____
Dean, Graduate School of **Natural and Applied Sciences**

Prof. Dr. Gönül Turhan Sayan _____
Head of Department, **Electrical and Electronics Engineering**

Assoc. Prof. Dr. Ali Özgür Yılmaz _____
Supervisor, **Electrical and Electronics Engineering Dept., METU**

Examining Committee Members:

Prof. Dr. Yalçın Tanık
Electrical and Electronics Engineering Department, METU _____

Assoc. Prof. Dr. Ali Özgür Yılmaz
Electrical and Electronics Engineering Department, METU _____

Prof. Dr. T. Engin Tuncer
Electrical and Electronics Engineering Department, METU _____

Assoc. Prof. Dr. Çağatay Candan
Electrical and Electronics Engineering Department, METU _____

Tuna Güven, Ph.D.
Lead Design Engineer, ASELSAN _____

Date: _____

I hereby declare that all information in this document has been obtained and presented in accordance with academic rules and ethical conduct. I also declare that, as required by these rules and conduct, I have fully cited and referenced all material and results that are not original to this work.

Name, Last Name: HALİL SAYGILI

Signature :

ABSTRACT

A COMPARISON OF SPATIAL MODULATION AND SPATIAL MULTIPLEXING SYSTEMS IN MULTIPATH FADING CHANNELS

Saygılı, Halil

M.S., Department of Electrical and Electronics Engineering

Supervisor : Assoc. Prof. Dr. Ali Özgür Yılmaz

September 2013, 75 pages

In this thesis, multiple antenna transmission techniques like spatial multiplexing, spatial modulation and multiple active spatial modulation are compared in multipath fading channels. Maximum likelihood sequence estimation (MLSE) based on the Ungerboeck observation model is the optimal operation for intersymbol interference channels and applied on the mentioned multiple antenna transmission strategies. The performance analysis based on Monte Carlo simulations and comparison of the computational complexity of the studied receiver structures showed us that spatial modulation has the lowest complexity and it can be an alternative to classical spatial multiplexing systems for low spectral efficiencies. But performance of spatial modulation starts to deteriorate for higher spectral efficiencies. In this case, multiple active spatial modulation is still a low complexity alternative for spatial multiplexing. Delayed decision feedback sequence estimation (DDFSE) based on the Ungerboeck model which is a suboptimal reduced state detection algorithm is also applied to these multiple antenna techniques. The performance analysis based on Monte Carlo simulations reveals that error propagation in DDFSE exacerbates the performance difference between spatial multiplexing and modulation.

Keywords: Spatial Modulation, Spatial Multiplexing, MLSE, DDFSE, Ungerboeck

ÖZ

ÇOK YOLLU SÖNÜMLEMELİ KANALLARDA UZAMSAL KİPLEME VE UZAMSAL ÇOĞULLAMA SİSTEMLERİNİN KARŞILAŞTIRILMASI

Saygılı, Halil

Yüksek Lisans, Elektrik ve Elektronik Mühendisliği Bölümü

Tez Yöneticisi : Doç. Dr. Ali Özgür Yılmaz

Eylül 2013 , 75 sayfa

Bu çalışmada, uzamsal çoğullama, uzamsal kipleme ve çoklu aktif uzamsal kipleme gibi çoklu anten aktarım teknikleri çok yollu sönümlemeli kanallarda karşılaştırılmıştır. Semboller arası girişimin oluştuğu kanallar için optimum kestirim algoritması olan Ungerboeck gözlemi tabanlı en büyük olabilirlikli dizi kestirimi (MLSE) yöntemi belirtilen çoklu anten tekniklerine uygulanmıştır. Monte Carlo simülasyonları ile yapılan performans analizleri ve önerilen alıcı yapılarının hesaplama karmaşıklığının kıyaslanması, uzamsal kiplemenin en düşük karmaşıklığa sahip olduğunu ve düşük spektral verimliliklerde klasik uzamsal çoğullama sistemlerine alternatif olabileceğini göstermiştir. Ancak uzamsal kiplemenin performansı artan spektral verimlilikler için kötüleşmeye başlamaktadır. Bu durumda, çoklu aktif uzamsal kipleme, uzamsal çoğullama için düşük karmaşıklığa sahip bir alternatif olmaya devam etmektedir. Azaltılmış durumlu optimal altı kestirim algoritması olan Ungerboeck gözlemi tabanlı gecikmeli karar geribildirimli dizi kestirimi (DDFSE) yöntemi de belirtilen çoklu anten tekniklerine uygulanmıştır. Monte Carlo simülasyonları ile yapılan başarım analizleri DDFSE yönteminin kullanıldığı durumda hata yayılımının uzamsal çoğullama ve kipleme arasındaki başarım farkını arttırdığını göstermektedir.

Anahtar Kelimeler: Uzamsal Kipleme, Uzamsal Çoğullama, MLSE, DDFSE, Ungerboeck

to my mother

ACKNOWLEDGMENTS

I would like to express my deepest gratitude to my supervisor Ali Özgür Yılmaz for his guidance and support throughout my graduate education and my thesis research. I am grateful to have the chance of working with him.

I would like to thank Professors Yalçın Tanık, T. Engin Tuncer and Çağatay Candan for being members of my thesis defense committee.

I would like to thank The Scientific and Technological Research Council of Turkey, TÜBİTAK, for their financial support during my graduate study.

I would like to thank my company ASELSAN Inc., for supporting my graduate study.

I would like to thank my manager Alper Gerçek for letting and supporting my graduate study. I would also like to thank my colleagues Dilek Erdemir, Tuna Güven, Zafer Arslanyürek, Atakan Aydın and Tuncay Taşdan for their collaboration, encouragement and support.

I wish to thank Koray Şen, İsmail Yaşar and Mehmet Mert for their valuable friendship.

Finally, I wish to thank my parents Habibe and Özdemir and my brother Serkan for their endless love and patience.

TABLE OF CONTENTS

LIST OF TABLES

TABLES

LIST OF FIGURES

FIGURES

CHAPTER 1

INTRODUCTION

Wireless communication systems that use multiple antenna transmission techniques are shown to achieve higher spectral efficiencies and smaller error rates compared to conventional single antenna systems [1,2]. Spectral efficiency can be increased by using spatial multiplexing techniques that provides multiplexing gain. The most famous spatial multiplexing technique is the BLAST structure proposed in [3,4]. In this structure, the data stream to be transmitted is demultiplexed into multiple substreams where no inter-substream coding is applied. Each substream is independently modulated and transmitted simultaneously from different transmit antennas and thus spectral efficiency increase linearly with the number of transmit antennas.

Spatial modulation is an alternative multiple-antenna transmission technique that increase spectral efficiency [5,6,7,8]. In spatial modulation only one antenna is active for transmission at a time in contrast to the classical multiple input multiple output techniques like BLAST or space-time coding. In spatial Modulation, the basic principle is modulating the symbol with not only phase or amplitude of the carrier but also with selection of the antenna for transmission of the carrier. The location of the activated antenna in spatial domain is used as an information source for transmission of data and thus spectral efficiency is increased.

Multiple active spatial modulation is a hybrid of spatial modulation and spatial multiplexing and uses multiple active transmit antennas with spatial modulation [9,10,11]. In this structure, the set of active antenna combinations is used an information source and each active antenna transmits different data streams. By doing that, spatial multiplexing is implemented on activated antennas and also spatial constellation points are used to convey information.

In literature, receiver structures like iterative-maximum ratio combining [5] and maximum likelihood decoder are proposed for spatial modulation [7]. For the BLAST structure, ZF or MMSE detector is used with successive interference cancellation and optimal ordering [4]. For multiple active spatial modulation, maximum likelihood decoder is proposed in [9,11]. The bit error rate performances of these receiver structures are compared for various configurations in flat fading channels in literature. In this study, we will analyze the capacity

behavior of the given multiple antenna techniques since such a capacity comparison does not exist in literature as far as we know.

Wireless communication channels have some serious problems to handle in high speed communications. One of them is multipath fading due to reflection, diffraction and scattering between transmitter and receiver [12,13]. Intersymbol Interference may occur according to the symbol rate and delay spread of the multipath channel. This problem can be solved optimally by using maximum likelihood sequence estimation (MLSE) at the receiver [14,15,16]. But computational complexity of MLSE grows exponentially with length of channel memory. In this situation using delayed decision feedback sequence estimation (DDFSE) may reduce the computational complexity significantly, but since DDFSE is not an optimal solution it may cause degradation in BER performance [17,18,19]. Hence, it offers a trade-off between performance and complexity.

In literature, receiver structures of spatial modulation are proposed for flat fading channels and does not consider multipath fading problem. In this study, we will propose optimal and suboptimal receiver structures for the mentioned multiple antenna techniques. We will compare the bit error rate performances and computational complexities and try to analyze trade-offs offered by the mentioned transmission strategies.

The outline of the thesis is as follows. In Chapter 2, channel impediments that exist in wireless communications is explained and channel models used in this work are described.

In Chapter 3, maximum likelihood sequence estimation which is the optimum detection algorithm for channels with intersymbol interference will be explained. Forney and Ungerboeck observation model approaches to this technique will be derived and compared using Monte Carlo simulations. Delayed decision feedback sequence estimation which is the suboptimum alternative of MLSE will also be considered in this chapter. DDFSE based on Forney and Ungerboeck observation models will also be derived and compared using Monte Carlo simulation method.

In Chapter 4, MIMO systems that increase spectral efficiency will be introduced. The transmitter structures of spatial multiplexing, spatial modulation and multiple active spatial modulation will be given. The capacity of the discrete memoryless channels for the given MIMO systems for uniformly distributed input constellations will be derived and compared using Monte Carlo simulations.

In Chapter 5, maximum likelihood sequence estimation based on Ungerboeck observation model will be applied on spatial multiplexing, spatial modulation and multiple active spatial modulation techniques. The reduced state suboptimal delayed decision feedback sequence estimation method based on Ungerboeck model is also applied to these multiple antenna techniques. For each receiver structure, computational complexity will be calculated and compared and bit error rate performances of the given MIMO systems are compared using Monte Carlo simulations.

The thesis concludes with Chapter 6.

CHAPTER 2

MODELING WIRELESS CHANNELS

2.1 The Wireless Channel

Wireless communication systems have to combat not only with noise which also exists in wireline communications but also with interference and fading [12,13,20,21]. In wireline communications, each transmitter and receiver pair can be considered as an isolated point to point link. In the wireless channel, there may be interference causes such as intersymbol interference for frequency selective channels, interchannel interference for multi-antenna systems and multi-user interference between wireless users. Each type of interference may occur separately as well as they may occur together. In addition to interference, the wireless channel has also other channel impediments that limit the performance of wireless communications like large scale and small scale fading.

Large-scale fading occurs due to path loss and shadowing. Path loss is the reduction in power density of the signal radiated by the transmitter due to the distance of the path between the transmitter and receiver [12,13]. In other words, path loss is the attenuation due to distance. Sometimes other losses such as atmospheric absorption are also effective but generally it is assumed that path loss is fixed for a given distance. So it can be considered as a deterministic parameter.

Shadowing is caused by obstacles such as buildings and hills between the transmitter and receiver which results in attenuation of received signal power [12,13]. Shadowing changes unpredictably due to location, size and dielectric properties of the blocking object, so it is generally considered as a random parameter.

Since attenuation due to path loss and shadowing occurs over very large distances and relatively big obstructing objects compared to signal wavelength, these impediments are considered as large scale effects.

Small-scale fading occurs due to the multipath phenomenon [12,13]. The transmitted signal will experience reflection, scattering, and diffraction in the wireless channel and, as a result, replicas of the transmitted signal arrive at the receive antenna with different phases and

amplitudes due to different delays and attenuations. In addition to that, if the transmitter or the receiver or the reflector is moving, the carrier frequency of the signal may increase or decrease according to the direction of the moving object. Echoes with different phases due to delay and Doppler effect can create constructive or destructive interference to each other when received at the receive antenna. Multipath effects change unpredictably due to user movement and environment dynamics so it is considered as a random parameter also. Large variations may occur due to multipath over very short distances compared to the signal wavelength, so these variations are considered as small scale effects.

Figure 2.1 illustrates the ratio of the received-to-transmit power in dB versus log-distance for the combined effects of path loss, shadowing, and multipath.

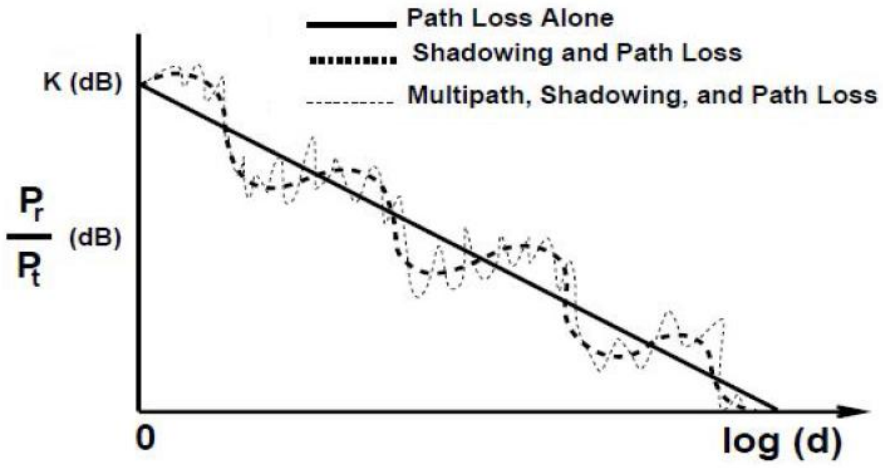

Figure 2.1: Path Loss, Shadowing and Multipath versus Distance [12]

2.2 Fading Channel Types

A model for the channel impulse response can be written as

$$h(t,\tau) = \sum_{l} h_l(t)\delta(t - \tau_l(t)) \tag{2.1}$$

where h_l and τ_l represent the channel path gain and delay for the l^{th} path, respectively [13].

The baseband equivalent signal representation of the generated signal over such a channel becomes

$$g(t) = \sum_l h_l(t) x(t - \tau_l(t)). \tag{2.2}$$

One of the parameters that shows the characteristic of the wireless channel is the delay spread. The delay spread equals the time difference between the arrivals of the first and the last received signals associated with the same transmitted signal:

$$T_m = \max_l \left| \tau_l - \tau_1 \right|. \tag{2.3}$$

If the reflectors are very close to each other then the delay differences between the paths will be small compared to the symbol duration and, as a result, individual paths cannot be distinguished. But when the delays between echoes are separated by more than the symbol duration, the individual paths become resolvable and intersymbol interference (ISI) occurs such that the delayed echoes of previous symbols interfere with the current symbol.

The delay spread approximately determines the coherence bandwidth of a frequency selective channel

$$B_c \approx \frac{1}{T_m}. \tag{2.4}$$

Complex amplitudes of spectral components of the channel response will be correlated in frequency range within a coherence bandwidth B_c and become uncorrelated at frequencies separated by more than B_c.

If the bandwidth of the signal is smaller than the coherence bandwidth of the channel then spectral components of the signal will experience same attenuations and such a channel will referred to as flat fading or frequency non-selective fading or narrowband channel.

If the bandwidth of the signal is larger than the coherence bandwidth of the channel then spectral components of the signal will experience different attenuations and such a channel will referred to as frequency selective or wideband channel.

Another parameter that shows the characteristic of a wireless channel is the Doppler spread. The Doppler spread equals to the maximum Doppler frequency shift due to relative movements of transmitter, receiver or reflector objects with the formula

$$B_d = \frac{v}{\lambda} \tag{2.5}$$

where v and λ represent the velocity of the moving object and wavelength of the signal, respectively.

The Doppler spread also determines the coherence time.

$$T_c \approx \frac{1}{B_d}. \tag{2.6}$$

The channel observed by the signal will be roughly static for the time duration denoted by coherence time and beyond T_c it starts to vary.

2.3 Time-Invariant Channel Model

In this thesis, each channel path gain is assumed to be time-invariant during transmission of a block of data and change to another independent value according to the statistical distribution for the next burst. The discrete-time baseband equivalent form of the received signal for a flat fading channel can be written as

$$y_k = hx_k + w_k. \tag{2.7}$$

The discrete-time baseband equivalent form of the received signal for a frequency selective fading channel can be written as

$$y_k = \sum_{l=0}^{L-1} h_l x_{k-l} + w_k, \tag{2.8}$$

where L denotes the length of overall channel impulse response and $L-1$ is the channel memory.

For each path, the channel path gain h_l is independently and identically distributed according to circularly symmetric complex Gaussian distribution with zero mean and variance $1/L$ which corresponds to the Rayleigh fading distribution.

Noise components are independently and identically distributed according to circularly symmetric complex Gaussian distribution with zero mean and variance N_0.

CHAPTER 3

SEQUENCE ESTIMATION BASED ON FORNEY AND UNGERBOECK MODELS

3.1 Maximum Likelihood Sequence Estimation

Maximum likelihood sequence estimation (MLSE) is the optimum detection algorithm for equiprobable sequences which are distorted by intersymbol interference and additive white Gaussian noise [14,15,16]. There are two classic approaches to maximum likelihood sequence estimation provided by Forney [14] and Ungerboeck [15].

In the receiver, matched filtering and sampling the received signal will produce sufficient statistics for estimation of the sequence [14,15]. But after matched filtering, the noise samples become correlated. In order to obtain white noise an invertible whitening filter should be used. Since the whitening filter is invertible, output samples of the filter are still sufficient statistics for estimation of the sequence. Forney's approach operates on samples of the output of the whitening filter while Ungerboeck's approach operates directly on samples of the output of the conventional matched filter.

The baseband portion of Forney's receiver is shown in Figure 3.1. Forney's receiver consists of a matched filter, a sampling operation, a whitening filter, and a sequence estimation algorithm such as the Viterbi algorithm. The algorithm operates on samples of the whitening filter output and uses the standard Euclidean distance metric since noise samples are white.

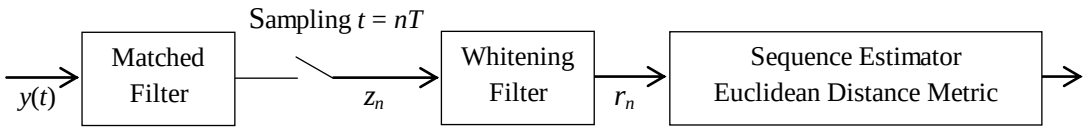

Figure 3.1: Forney's Receiver

The baseband portion of Ungerboeck's receiver is shown in Figure 3.2. Ungerboeck's receiver consists of a matched filter, a sampling operation, and a sequence estimation algorithm such as the Viterbi algorithm. The algorithm operates on samples of the conventional matched filter output and uses a modified distance metric since noise samples are correlated.

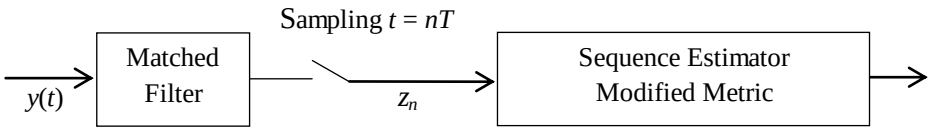

Figure 3.2: Ungerboeck's Receiver

The system model consists of a transmitter, a linear dispersive transmission medium, and a receiver. The baseband equivalent of the received signal for a complex information symbol sequence $\{x_n\}$ which passes through a linear time-invariant channel with impulse response $h(\tau)$ is given as

$$y(t) = \sum_n x_n h(t - nT) + w(t), \tag{3.1}$$

where $w(t)$ is additive white Gaussian noise (AWGN). The received signal $y(t)$ is collected over a finite time interval denoted by I which is supposed to be long enough. The channel is assumed to be known at the receiver.

3.2 MLSE Based on Ungerboeck Model

The MLSE receiver finds the sequence of data symbols $\{x_n\}$ that maximizes the likelihood function obtained from the a posteriori distribution of the received signal $y(t)$ conditioned on the transmitted sequence $\{x_n\}$ [14,15,16]. After neglecting constant scaling factors and additive terms in the log-likelihood function, maximizing the log-likelihood function will be equivalent to maximizing

$$\begin{aligned} PM(\{x_n\}) &= -\int_{t\in I} \left| y(t) - y(t) \right|^2 dt \\ &= -\int_{t\in I} \left| y(t) - \sum_n x_n h(t - nT) \right|^2 dt \end{aligned} \tag{3.2}$$

where $\tilde{y}(t)$ is the signal which is formed by using the knowledge of the channel and a hypothesis of the transmitted symbol sequence $\{x_n\}$ and PM is the path metric corresponding to this hypothesis.

The path metric can be expanded as

$$PM(\{x_n\}) = -\int_{t\in I}\left[y(t) - \sum_n x_n h(t-nT) \right]^* \left[y(t) - \sum_n x_n h(t-nT) \right] dt$$

$$= A + B(\{x_n\}) + C(\{x_n\}) \tag{3.3}$$

where

$$A = -\int_{t\in I} |y(t)|^2 dt \tag{3.4}$$

$$B(\{x_n\}) = \int_{t\in I} 2\,\mathrm{Re}\left\{ \sum_n x_n^* h^*(t-nT) y(t) \right\} dt \tag{3.5}$$

$$C(\{x_n\}) = -\int_{t\in I} \sum_n \sum_k x_n^* x_k h^*(t-nT) h(t-kT) dt. \tag{3.6}$$

Since term A is independent of the hypothesis of the symbol sequence $\{x_n\}$ and common to all metrics, it can be omitted. Interchanging the order of integration with summation in (3.5) and (3.6) will result in

$$B(\{x_n\}) = 2\,\mathrm{Re}\left\{ \sum_n x_n^* z_n \right\} \tag{3.7}$$

$$C(\{x_n\}) = -\sum_n \sum_k x_n^* x_k g_{n-k} \tag{3.8}$$

where

$$z_n = \int_{t\in I} h^*(t-nT) y(t) dt \tag{3.9}$$

$$g_{n-k} = \int_{t+nT\in I} h^*(t) h(t+(n-k)T) dt. \tag{3.10}$$

Sequence $\{z_n\}$ represents the symbols sampled at the output of the matched filter at the symbol rate 1/T. The filter is matched to the channel impulse response $h(\tau)$ and has an impulse response $h^*(-\tau)$. Sequence $\{g_{n-k}\}$ represents the samples of autocorrelation function of $h(\tau)$, taken periodically at 1/T and has the following property

$$g_{k-n} = g_{n-k}^*. \tag{3.11}$$

The double summation can also be written as

$$\sum_r \sum_c a_{rc} = \sum_r a_{rr} + \sum_r \sum_{c<r} [a_{rc} + a_{cr}]. \tag{3.12}$$

Using the statements given in (3.11) and (3.12), the term in (3.8) can be rewritten as

$$C(\{x_n\}) = -\sum_n x_n^* x_n g_0 - \sum_n \sum_{k<n} [x_n^* x_k g_{n-k} + x_k^* x_n g_{k-n}]$$

$$= -\sum_n x_n^* x_n g_0 - \sum_n \sum_{k<n} [x_n^* x_k g_{n-k} + x_n x_k^* g_{n-k}^*]$$

$$= -\sum_n x_n^* x_n g_0 - \sum_n \sum_{k<n} 2\,\mathrm{Re}\{x_n x_k^* g_{n-k}^*\}. \tag{3.13}$$

After making a change of variable $l=n-k$ for the second term, $C(\{x_n\})$ becomes

$$C(\{x_n\}) = -\sum_n x_n^* x_n g_0 - \sum_n \sum_{l>0} 2\,\mathrm{Re}\{x_n^* x_{n-l} g_l\}. \tag{3.14}$$

If the length of the channel impulse response is L which means that length of the channel memory is $L-1$, the autocorrelation function will satisfy

$$g_l = 0 \quad \text{for } |l| > L-1. \tag{3.15}$$

Finally the path metric can be rewritten according to (3.7), (3.14) and (3.15)

$$PM(\{x_n\}) = \sum_n \mathrm{Re}\left\{ x_n^* \left[2z_n - g_0 x_n - 2\sum_{l=1}^{L-1} x_{n-l} g_l \right] \right\}. \tag{3.16}$$

The path metric can be defined as the sum of branch metrics as

$$PM(\{x_n\}) = \sum_n BM_n \tag{3.17}$$

where the branch metric is defined as

$$BM_n = \mathrm{Re}\left\{ x_n^* \left[2z_n - g_0 x_n - 2\sum_{l=1}^{L-1} x_{n-l} g_l \right] \right\}. \tag{3.18}$$

As a conclusion, Ungerboeck's approach uses samples of matched filter outputs directly to calculate the part metric. The sequence of information symbols $\{x_n\}$ which maximizes the path metric is chosen as the estimate.

3.3 MLSE Based on Forney Model

Forney's receiver model can be obtained by simply extending Ungerboeck's receiver model by using a whitening filter. Output samples of the matched filter can be rewritten by substituting (3.1) in (3.9) as

$$\begin{aligned} z_n &= \int_{t\in I} h^*(t-nT)\, y(t)\, dt \\ &= \int_{t\in I} h^*(t-nT) \sum_k x_k h(t-kT)\, dt + \int_{t\in I} h^*(t-nT)\, w(t)\, dt \\ &= \sum_k x_k \int_{t\in I} h^*(t-nT) h(t-kT)\, dt + u_n \\ &= \sum_k x_k g_{n-k} + u_n. \end{aligned} \tag{3.19}$$

Output samples of the matched filter can also be expressed alternatively as

$$z_n = \sum_{l=-(L-1)}^{L-1} g_l x_{n-l} + u_n \tag{3.20}$$

where

$$u_n = -\int_{t \in I} h^*(t - nT) w(t) dt. \tag{3.21}$$

Let $G(z)$ denote the z-transform of the sampled autocorrelation function $\{g_l\}$.

$$G(z) = \sum_{l=-(L-1)}^{L-1} g_l z^{-l}. \tag{3.22}$$

Equation (3.11) denotes that $g_l = g_{-l}^*$ so the z-transform $G(z)$ has the property

$$G(z) = G^*\left(\frac{1}{z^*}\right) \tag{3.23}$$

and the $2(L-1)$ roots of $G(z)$ have the symmetry such that if ρ is a root then $1/\rho^*$ is also a root. According to this fact, $G(z)$ can be factored as

$$G(z) = F(z) F^*\left(\frac{1}{z^*}\right) \tag{3.24}$$

and the inverse z-transform gives the discrete convolution

$$g_l = \sum_d f_{l-d} f_{-d}^* = \sum_p f_p f_{p-l}^* \tag{3.25}$$

The correlated noise sequence $\{u_n\}$ has an autocorrelation function of the form

$$E\{u_n u_{n-l}^*\} = N_0 g_l. \tag{3.26}$$

The correlated noise sequence $\{u_n\}$ can be generated by passing a white noise sequence $\{v_n\}$ through a filter whose *z*–transformed impulse response is $F^*(1/z^*)$

$$u_n = \sum_d f_{-d}^* v_{n-d}. \tag{3.27}$$

Output samples of the matched filter can be rewritten by substituting (3.25) and (3.27) in (3.19) as

$$\begin{aligned} z_n &= \sum_k x_k g_{n-k} + u_n \\ &= \sum_k x_k \sum_d f_{n-i-d} f_{-d}^* + \sum_d f_{-d}^* v_{n-d} \end{aligned} \tag{3.28}$$

and after making a change of variable as $p = n\text{-}d$, samples of matched filter output become

$$\begin{aligned} z_n &= \sum_k x_k \sum_p f_{p-k} f_{p-n}^* + \sum_p f_{p-n}^* v_p \\ &= \sum_p f_{p-n}^* \left[\sum_k x_k f_{p-k} + v_p \right]. \end{aligned} \tag{3.29}$$

The term $B(\{x_n\})$ in the path metric can be rewritten by substituting (3.29) into (3.7) as in

$$\begin{aligned} B(\{x_n\}) &= 2\,\mathrm{Re}\left\{ \sum_n x_n^* z_n \right\} \\ &= 2\,\mathrm{Re}\left\{ \sum_n x_n^* \sum_p f_{p-n}^* \left[\sum_k x_k f_{p-k} + v_p \right] \right\} \\ &= 2\,\mathrm{Re}\left\{ \sum_p \sum_n x_n^* f_{p-n}^* \left[\sum_k x_k f_{p-k} + v_p \right] \right\} \\ &= 2\,\mathrm{Re}\left\{ \sum_p \tilde{r}_p^* r_p \right\} \end{aligned} \tag{3.30}$$

where

$$r_p = \sum_k x_k f_{p-k} + v_p \tag{3.31}$$

$$\tilde{r}_p = \sum_n x_n f_{p-n}. \tag{3.32}$$

The term $C(\{x_n\})$ in the path metric can be rewritten by substituting (3.25) into (3.8) as

$$C(\{x_n\}) = -\sum_p \left|\tilde{r}_p\right|^2. \tag{3.33}$$

The path metric is defined as the summation of terms $B(\{x_n\})$ and $C(\{x_n\})$ which are given in (3.30) and (3.33). Adding a constant term, which is independent of the hypothesis of the symbol sequence $\{x_n\}$, will not change the maximization problem. Hence, adding the term $|r_p|^2$ which is accumulated over p to the summation of the terms in (3.30) and (3.33), the path metric can be rewritten as

$$PM(\{x_n\}) = -\sum_p \left|r_p - \tilde{r}_p\right|^2. \tag{3.34}$$

The maximization problem can be turned into a minimization problem by simply removing the minus sign at the beginning of the expression.

As a summary, after matched filtering and sampling of the received signal $y(t)$, the discrete time sequence $\{z_n\}$ is obtained and its z-transform is given by

$$Z(z) = \sum_k x_k z^{-k} F(z) F^*(\frac{1}{z^*}) + V(z) F^*(\frac{1}{z^*}) \tag{3.35}$$

The matched filter outputs pass through the whitening filter which has the response given by $1/F^*(1/z^*)$. The outputs of the whitening filter is the discrete time sequence $\{r_p\}$ and its z-transform is given by

$$R(z) = \frac{Z(z)}{F^*(\frac{1}{z^*})} = \sum_k x_k z^{-k} F(z) + V(z). \tag{3.36}$$

In the discrete time domain, the output of the whitening filter can be expressed alternatively as

$$r_n = \sum_{l=0}^{L-1} f_l x_{n-l} + v_n. \tag{3.37}$$

Finally, the discrete time sequence $\{r_n\}$ is used for calculation of the path metric which is a standard Euclidean distance metric. The sequence of information symbols $\{x_n\}$ which maximizes the path metric is chosen as the estimate. For sequence estimation, an efficient method which is called the Viterbi algorithm is often used [22].

3.4 The Viterbi Algorithm

The Viterbi algorithm is an optimal recursive nonlinear algorithm which can be used for sequence estimation [22]. Complexity of the brute force ML estimation is exponential in the length of data sequence. The Viterbi algorithm offers a complexity which is exponential only in the length of channel memory.

In order to compute the branch metric at time n for a hypothetical sequence of information symbols $\{x_n\}$, a current symbol x_n and a state σ_n consisting of the past $L-1$ symbols are used.

$$\sigma_n = (x_{n-1}, x_{n-2}, ..., x_{n-(L-1)}). \tag{3.38}$$

Using (3.18), the branch metrics for state transitions can be computed based on Ungerboeck formulation as

$$BM_n = BM(x_n, \sigma_n) = BM(\sigma_n \to \sigma_{n+1}) = \mathrm{Re}\left\{ x_n^* \left[2z_n - g_0 x_n - 2\sum_{l=1}^{L-1} x_{n-l} g_l \right] \right\}. \tag{3.39}$$

Since there is a one to one correspondence between states and sequences, the optimum sequence can be found by selecting the optimum path through a trellis representing the states and transitions. The Trellis diagram of a BPSK signalling in a 3-tap ISI channel is depicted in Figure 3.3. The solid line indicates the transition if the current input is +1, while the dashed line indicates the transition if the current input is -1.

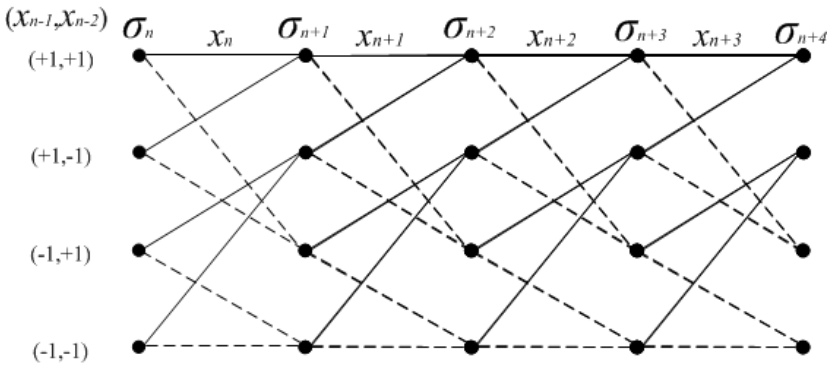

Figure 3.3: Trellis diagram of BPSK signalling in a 3-tap ISI channel

If x_n is a symbol chosen from an alphabet with size M, then the number of possible states is M^{L-1}. For each state there are M possible transitions which mean that there are M^L possible transitions in total at a time epoch n.

Since any number of sequences at a state can be directly compared, the sequence with the largest sum will be chosen as the surviving branch for that state and the other branches should be discarded. Since there are M^{L-1} possible states at time n, there will be M^{L-1} survivors which we have to track. After following this algorithm for each state, the path with the best metric should be picked at the end. The Viterbi algorithm can be applied to both the Forney and Ungerboeck observation models. The only difference is in the formulation for calculation of the branch metrics.

In the following figures, the bit error rate (BER) performances of the models are investigated based on Monte Carlo simulations. As mentioned earlier, each channel path gain is assumed to be time-invariant during transmission of a block of data and change to another independent value according to the statistical distribution for the next burst. In the simulations, each block to be transmitted in a burst has a length of 500 bits and each simulation was run for a count of 10000 bit errors.

The performance of maximum likelihood sequence estimation based on Forney and Ungerboeck observation models for BPSK signalling $x_n \in \{+1,-1\}$ and QPSK signalling $x_n \in \{+1, j, -1, -j\}$ in 2-tap, 3-tap and 4-tap ISI channels are depicted in Figures 3.4 - 3.9. As expected, both models show identical performance for sequence estimation with full state trellis search.

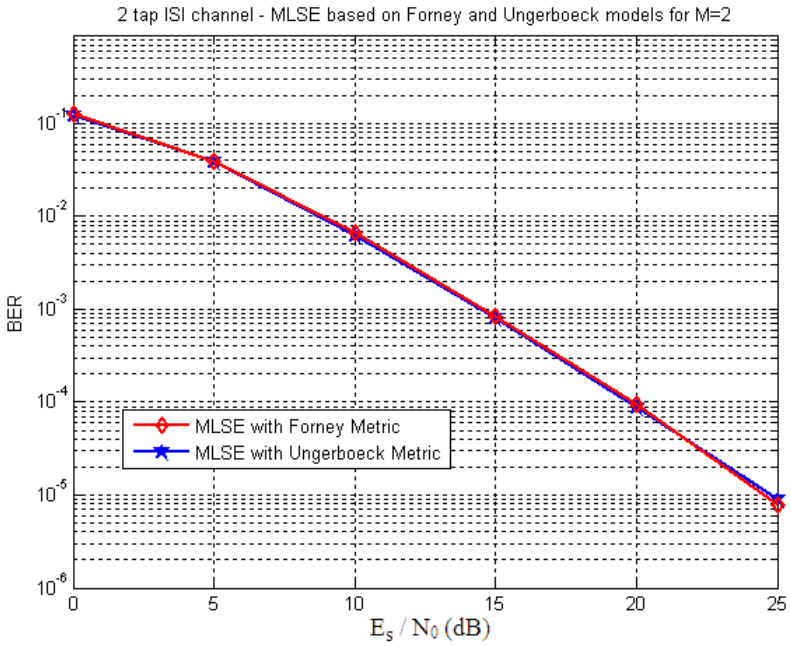

Figure 3.4: MLSE based on Forney and Ungerboeck models for BPSK signalling in 2-tap ISI channel

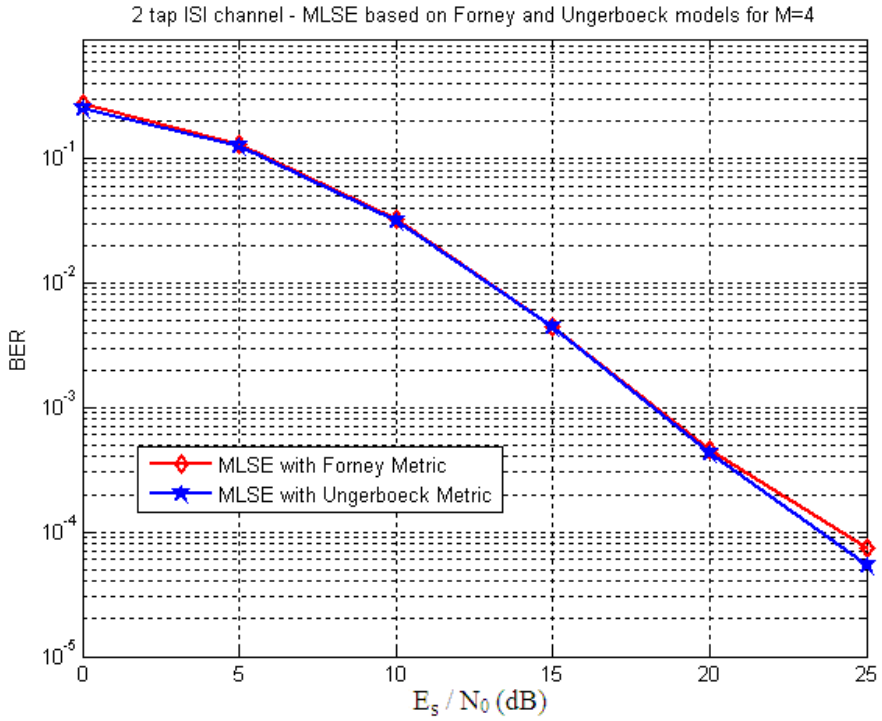

Figure 3.5: MLSE based on Forney and Ungerboeck models for QPSK signalling in 2-tap ISI channel

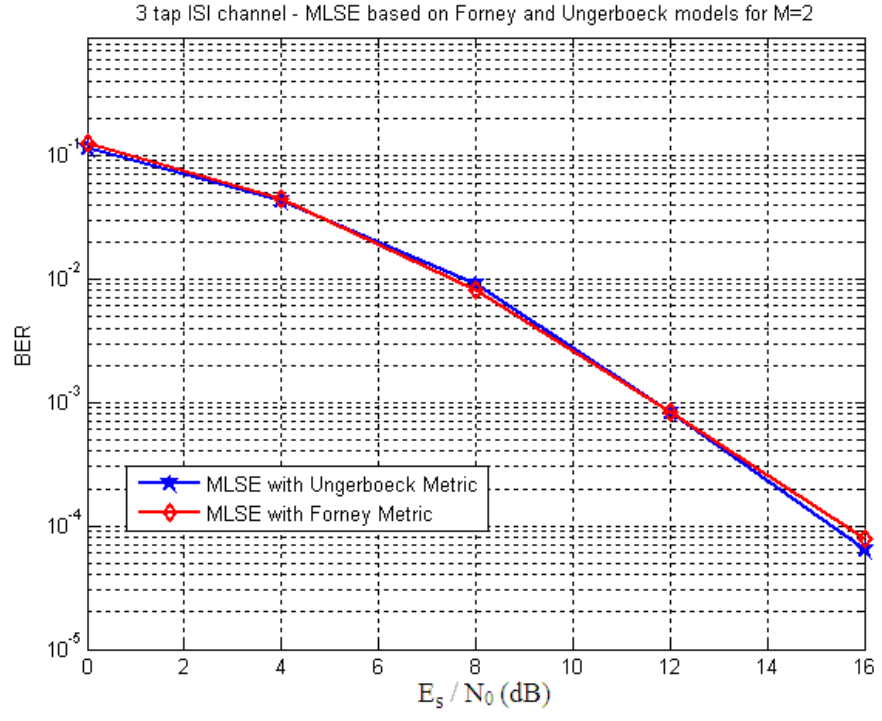

Figure 3.6: MLSE based on Forney and Ungerboeck models for BPSK signalling in a 3-tap ISI channel

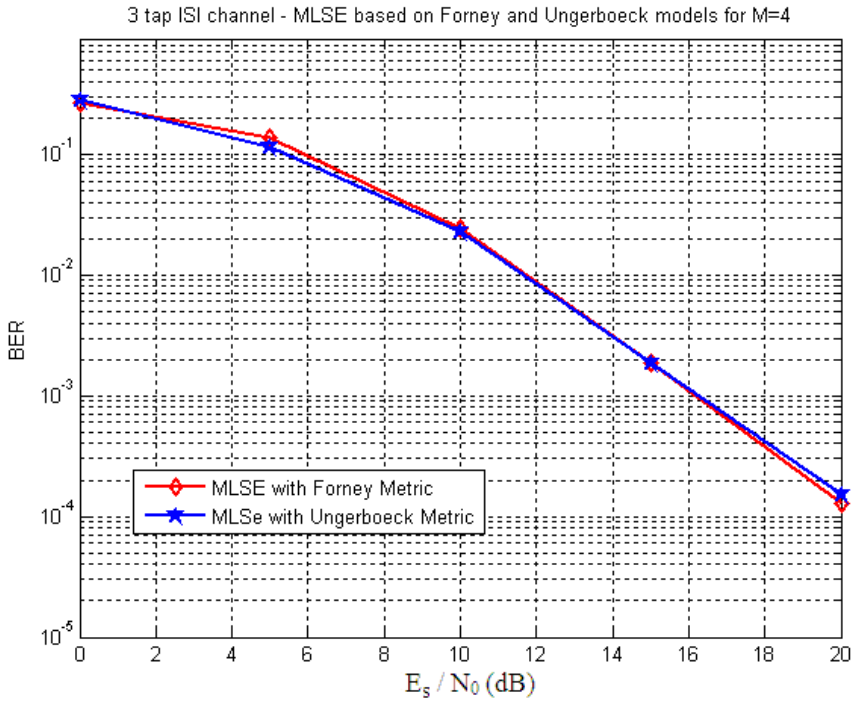

Figure 3.7: MLSE based on Forney and Ungerboeck models for QPSK signalling in a 3-tap ISI channel

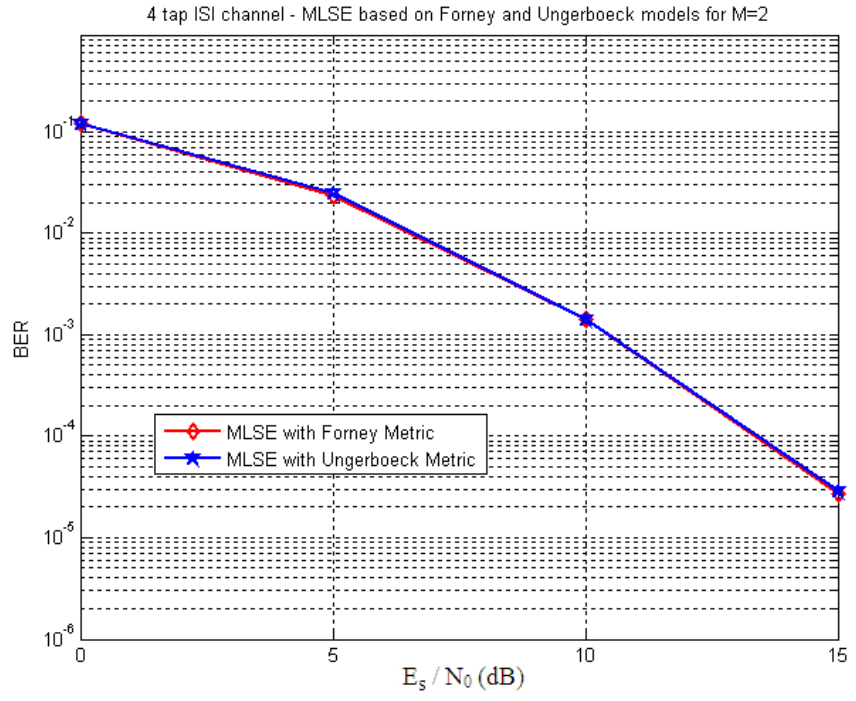

Figure 3.8: MLSE based on Forney and Ungerboeck models for BPSK signalling in a 4-tap ISI channel

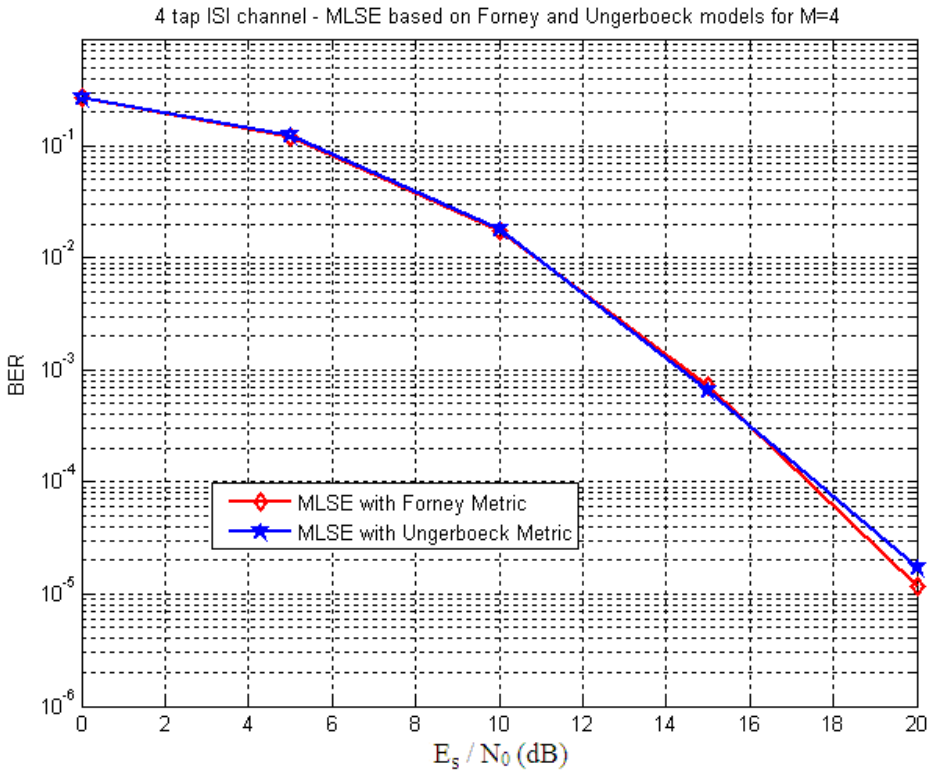

Figure 3.9: MLSE based on Forney and Ungerboeck models for QPSK signalling in a 4-tap ISI channel

3.5 Delayed Decision Feedback Sequence Estimation

The maximum likelihood sequence estimation based on Forney or Ungerboeck observation model is the optimum detection algorithm for intersymbol interfence channels with additive white Gaussian noise as explained previously. The Viterbi algorithm provides an efficient method without loss of optimality. The number of states and branch metric calculations in the trellis grow exponentially with the length of the channel memory. For channels with long memory, the structure becomes too complex.

Due to the exponential complexity of MLSE, several low-complexity suboptimal schemes have been considered in literature. Delayed decision feedback sequence estimation (DDFSE) method given in [17,18] is a reduced complexity suboptimal alternative for MLSE based on Forney's approach. The trade-off between complexity and performance is controlled by a parameter J which is called as the memory order. Memory order J can be chosen between zero and the length of the channel memory $L-1$. States are defined based on past J symbols so number of states for an M-ary alphabet is equal to M^J.

By choosing memory order smaller than the length of the channel memory, we obtain a reduced state trellis but this method is different from directly truncating the channel memory such that the estimates of the remaining past symbols from *J+1* to *L-1* are also used in calculating the branch metrics. The estimates of past symbols can be obtained by tracking the surviving path leading to each state.

In the classical Decision Feedback Equalization technique, the intersymbol interference for the current symbol is canceled by using the estimates of past symbols without using any trellis structure [23]. From this point of view, DDFSE can be considered as a hybrid of DFE and MLSE. If the memory order is chosen as zero than the algorithm turns into decision feedback estimation and if the memory order is chosen as the length of the channel memory than the algorithm performs maximum likelihood sequence estimation.

The branch metric for DDFSE based on the Forney metric (considered as minimization problem) is given as

$$BM_n = \left| r_n - \sum_{l=0}^{J} f_l x_{n-l} - \sum_{l=J+1}^{L-1} f_l \hat{x}_{n-l} \right|^2 \tag{3.40}$$

where (x_{n-1}, x_{n-2},…, x_{n-J}) are considered as the symbols that make up the state in trellis and ($\hat{x}_{n-J-1}$, $\hat{x}_{n-J-2}$,…, $\hat{x}_{n-L+1}$) are considered as feedback of the decided symbols which are obtained by tracking the surviving path leading to that state.

DDFSE based on Forney metric has a weakness such that its performance is sensitive to type of channel obtained after whitening filter. It shows the best performance for minimum phase channels but performance decreases for nonminimum phase channels.

Delayed decision feedback sequence estimation as a reduced state suboptimal alternative to MLSE based on Ungerboeck's approach is considered in [19]. The only difference is that the algorithm operates directly on discrete-time unwhitened samples which are samples of the conventional matched filter output. DDFSE based on Ungerboeck model is robust to the type of the ISI channel.

The branch metric for DDFSE based on the Ungerboeck metric (considered as maximization problem) is given as

$$BM_n = \mathrm{Re}\left\{ x_n^* \left[2z_n - g_0 x_n - 2\sum_{l=1}^{J} g_l x_{n-l} - 2\sum_{l=J+1}^{L-1} g_l \hat{x}_{n-l} \right] \right\} \tag{3.41}$$

where (x_{n-1}, x_{n-2},…, x_{n-J}) are considered as the symbols that make up the state in trellis and ($\hat{x}_{n-J-1}$, $\hat{x}_{n-J-2}$,…, $\hat{x}_{n-L+1}$) are considered as feedback of the decided symbols which are obtained by tracking the surviving path leading to that state.

Since the channel taps are independently distributed, they are not necessarily minimum or maximum phase. We like to show here that Ungerboeck model based receivers are robust as opposed to Forney model based receivers.

In the following figures, the bit error rate (BER) performances of the models are investigated using Monte Carlo simulation method. As mentioned earlier, each channel path gain is assumed to be time-invariant for each burst. In the simulations, each block to be transmitted in a burst has a length of 500 bits and each simulation was run for a count of 10000 bit errors.

The performance of delayed decision feedback sequence estimation based on Forney and Ungerboeck observation models for BPSK signalling $x_n \in \{+1,-1\}$ and QPSK signalling $x_n \in \{+1, j, -1, -j\}$ in 3-tap and 4-tap ISI channels are depicted in Figures 3.10 - 3.15. The memory order is chosen as $J=1$ for 3-tap ISI channel. For 4-tap ISI channel, both $J=1$ and $J=2$ configurations are considered. As seen in the figures, DDFSE based on Ungerboeck model is superior to DDFSE based on Forney model for the given configurations.

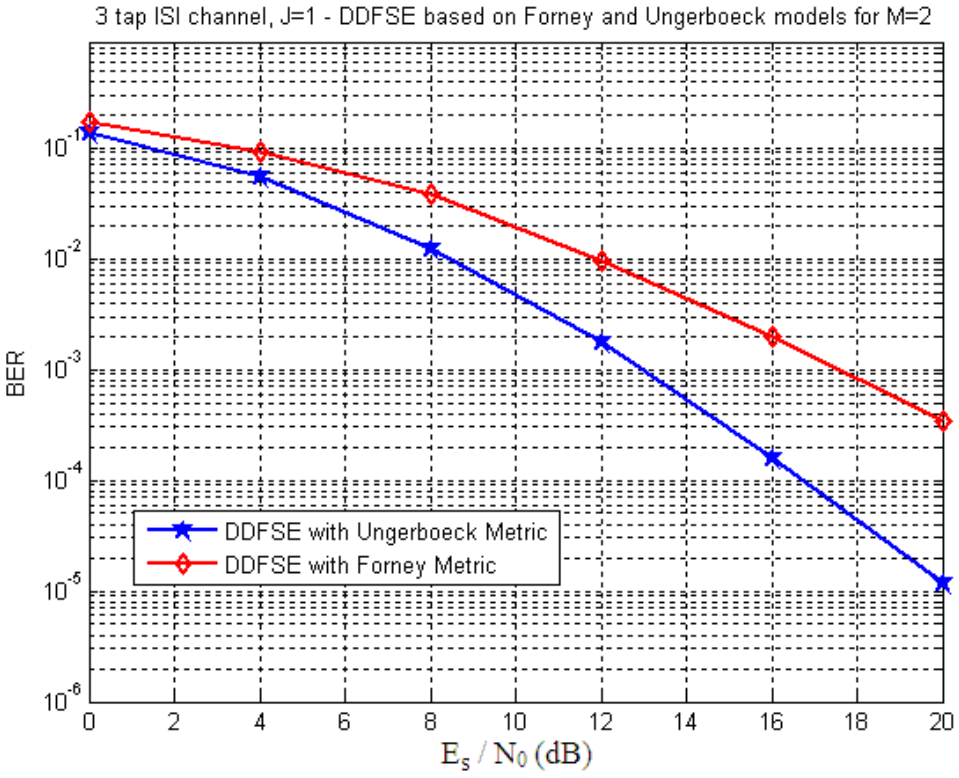

Figure 3.10: DDFSE based on Forney and Ungerboeck models for BPSK signalling in a 3-tap ISI channel with memory order $J=1$

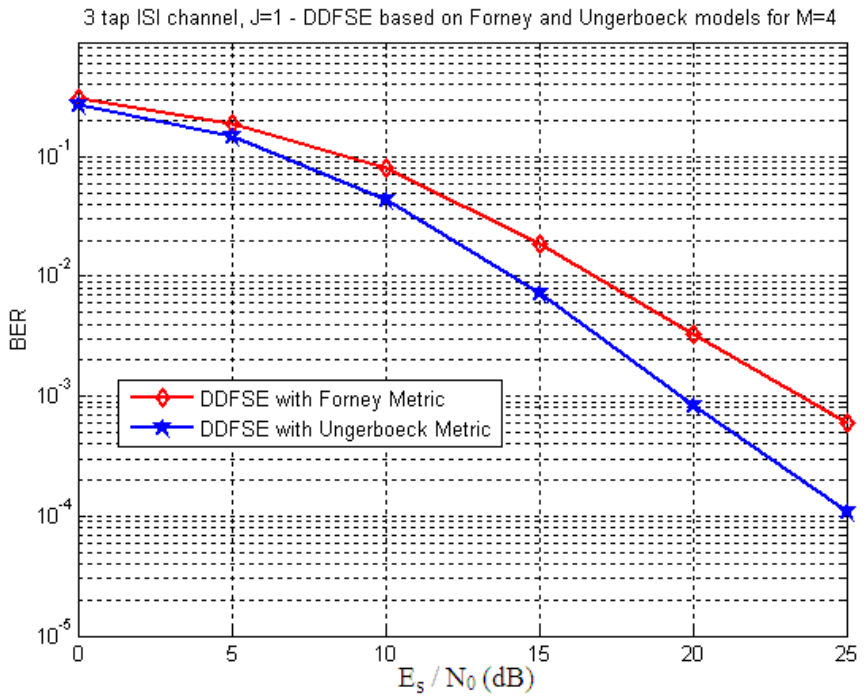

Figure 3.11: DDFSE based on Forney and Ungerboeck models for QPSK signalling in a 3-tap ISI channel with memory order J=1

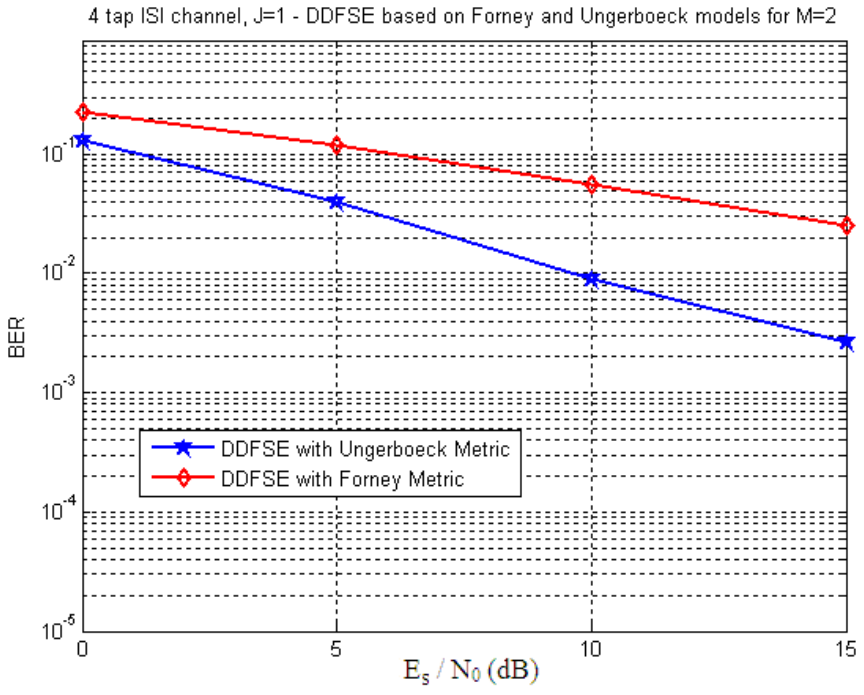

Figure 3.12: DDFSE based on Forney and Ungerboeck models for BPSK signalling in a 4-tap ISI channel with memory order J=1

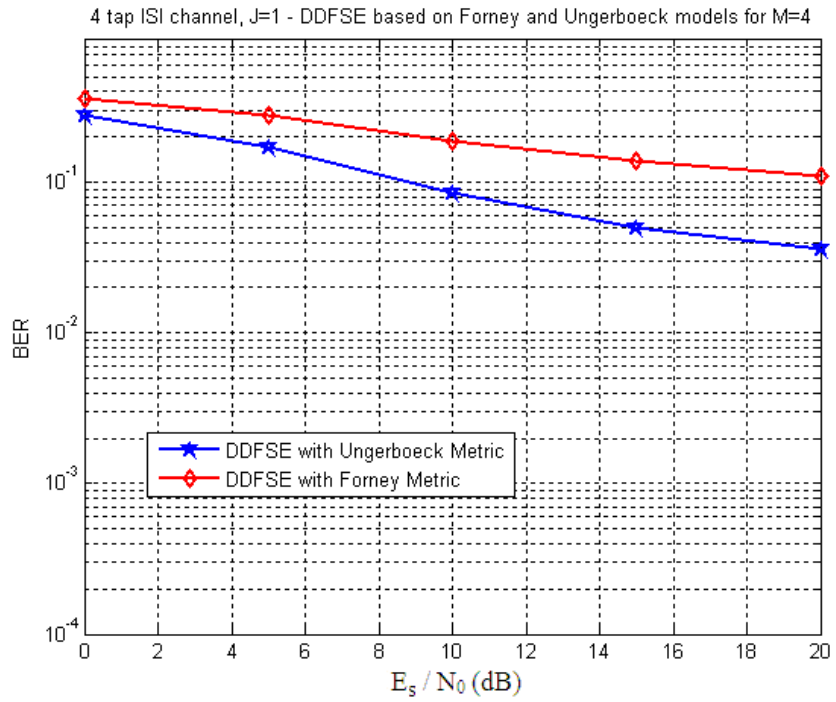

Figure 3.13: DDFSE based on Forney and Ungerboeck models for QPSK signalling in a 4-tap ISI channel with memory order J=1

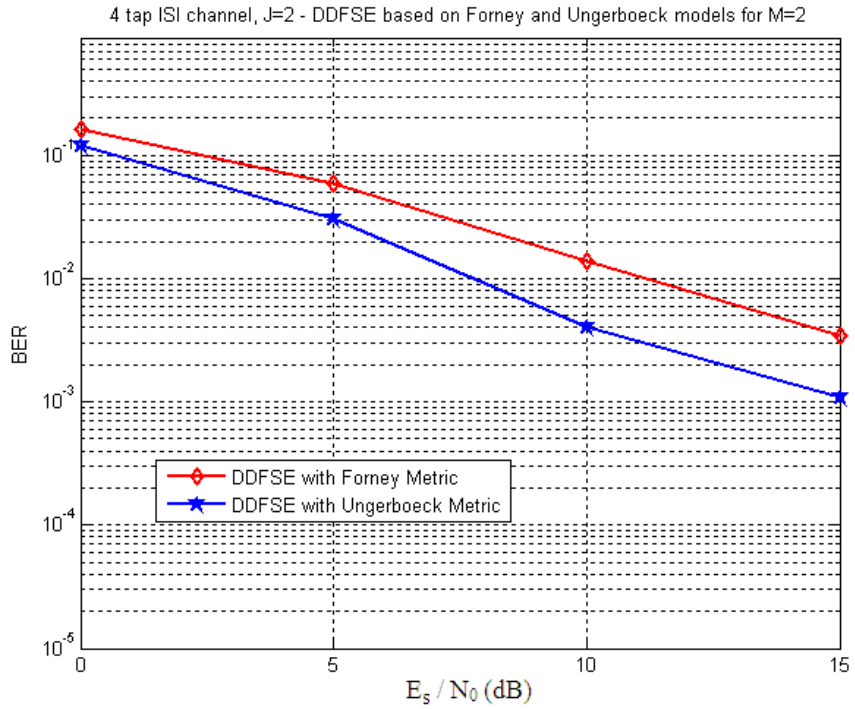

Figure 3.14: DDFSE based on Forney and Ungerboeck models for BPSK signalling in a 4-tap ISI channel with memory order J=2

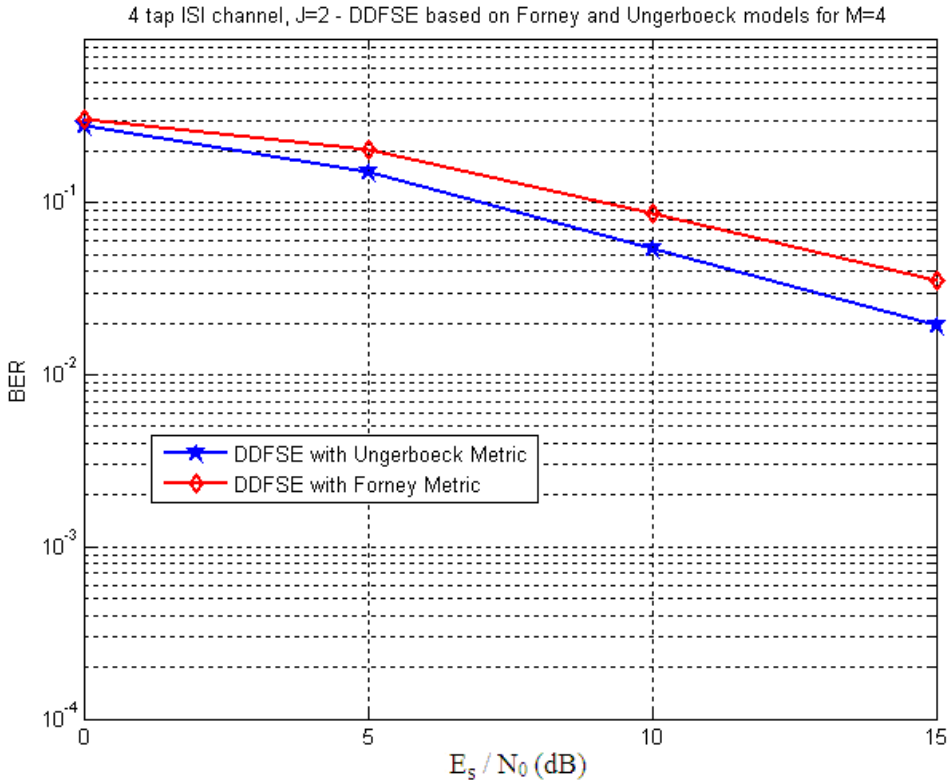

Figure 3.15: DDFSE based on Forney and Ungerboeck models for QPSK signalling in a 4-tap ISI channel with memory order J=2

In this section, we compared two classical approaches for sequence estimation which are called as Forney and Ungerboeck observation models. Forney's formulation for branch metric calculation depends directly on coefficients of channel obtained after whitening filter which means that Forney's metric is sensitive to type and phase of channel which can be considered as a weakness. Ungerboeck's formulation for branch metric calculation depends on output of the matched filter and autocorrelation function of channel which means that Ungerboeck's metric is insensitive to phase of channel. The simulation results indicate that both models show identical performances when MLSE is applied since it makes a full state trellis search. The simulation results also indicate that there is a performance difference between observation models when DDFSE is applied since performance of DDFSE based on Forney model deteriorates for nonminimum phase channels. Also DDFSE based on Ungerboeck model eliminates the need to calculate a whitening filter. Due to these benefits, DDFSE based on Ungerboeck model is preferable for suboptimal case which is of interest in this thesis.

CHAPTER 4

MIMO SYSTEMS AND SPATIAL MODULATION

4.1 MIMO Systems

The simplest configuration of the wireless systems is using a single antenna for both the transmitter and the receiver as shown in Figure 4.1. This configuration is called single input single output (SISO) system.

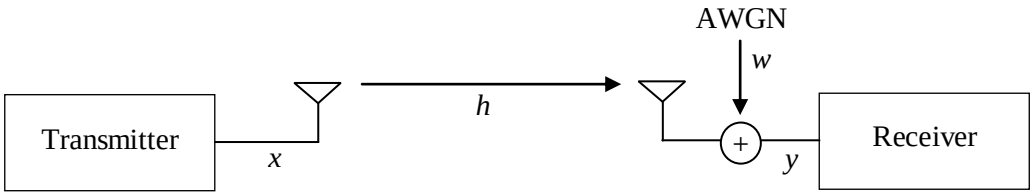

Figure 4.1: SISO System Model

Multiple antennas can be used at the transmitter, receiver or at both sides in order to increase reliability and spectral efficiency of wireless communication systems [2]. Data rates of wireless communication systems can be increased by using spatial multiplexing techniques that provides multiplexing gain and smaller error rates can be obtained by using spatial diversity techniques that provides diversity gain [2].

The systems that use multiple antennas at the receiver side only are called single input multiple output (SIMO) systems. SIMO systems are generally used to obtain receive diversity by using techniques like selection combining, maximal ratio combining, or equal gain combining.

The SIMO system model is shown in Figure 4.2.

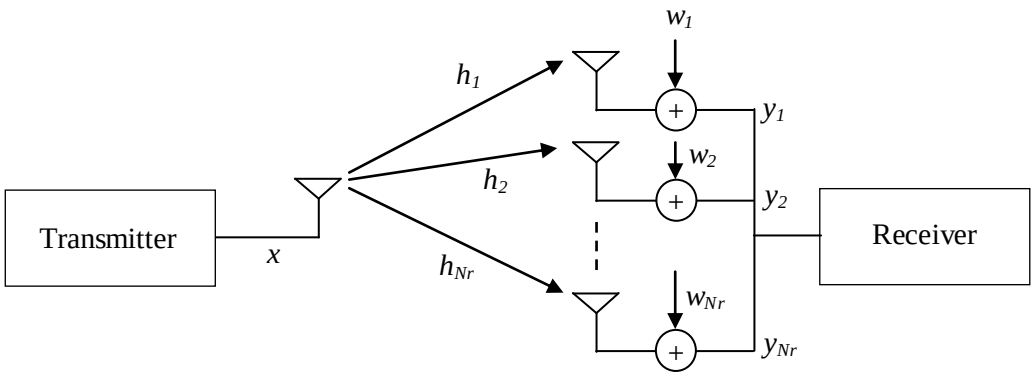

Figure 4.2: SIMO System Model

The simplest receive diversity technique is selecting the branch with the highest SNR as the output signal which is called selection combining [24]. Maximal ratio combining aims to maximize SNR by multiplying the branches with weighting factors and making phase and gain adjustment [24]. But sometimes SNR on each branch is unknown so adjustment is done only according to the phase. This technique called equal gain combining [24].

The systems that use multiple antennas only at the transmitter side are called multiple input multiple output (MISO) systems. MISO systems are generally used to obtain transmit diversity by using techniques like space time coding, space frequency coding, etc.

The MISO system model is shown in Figure 4.3.

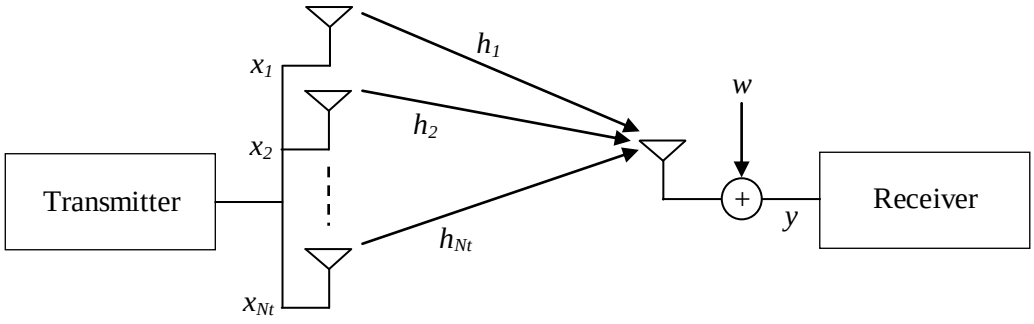

Figure 4.3: MISO System Model

In space time coding, the spacing between transmit antennas are set sufficiently apart that the channel path gains for different transmit antennas are uncorrelated. The modified replicas of the symbols transmitted from antennas are sent over different time slots to obtain diversity [25]. Space frequency coding is similar to space time coding but diversity is obtained by using different carriers instead of time slots [26].

The systems that use multiple antennas at both the transmitter and the receiver side are called multiple input multiple output (MIMO) systems. MIMO systems can be used for obtaining both transmit and receive diversity gain as well as they can be used for obtaining multiplexing gain and increasing spectral efficiency.

The MIMO system model is shown in Figure 4.4.

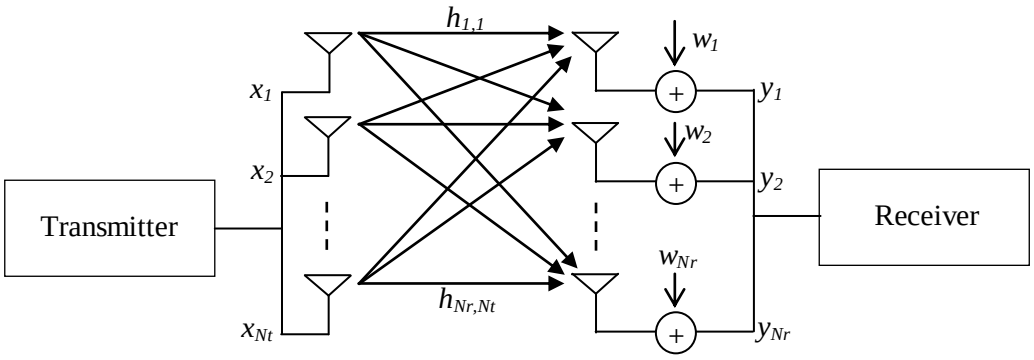

Figure 4.4: MIMO System Model

In this thesis, we are focusing on MIMO techniques that increase spectral efficiency such as spatial multiplexing, spatial modulation and multiple active spatial modulation.

4.2 Spatial Multiplexing

Spatial multiplexing is a multiple antenna transmission technique that transmits multiple data streams from transmit antennas to increase spectral efficiency of wireless communication systems. The most famous spatial multiplexing technique is the BLAST structure proposed in [3,4].

In the BLAST structure, the transmission vector encoding process is a demultiplexing operation. The data stream to be transmitted is demultiplexed into N_t substreams where no inter-substream coding is applied. Each substream is independently modulated according to same *M*-ary QAM/PSK constellation and transmitted simultaneously from different transmitter antennas over the same frequency band. Spectral efficiency is increased linearly with the number of transmit antennas. This gain is referred to as multiplexing gain. The transmitter structure of BLAST is shown in Figure 4.5.

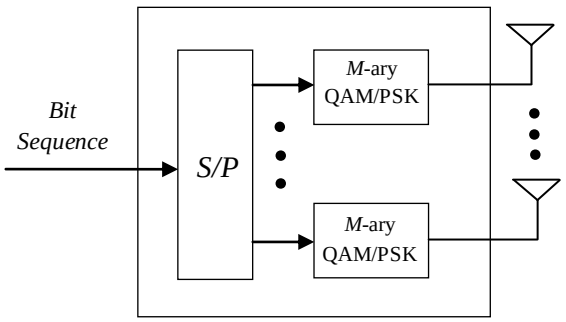

Figure 4.5: Transmitter structure of BLAST

The number of bits that are mapped into the transmit signal vector **x** is given by

$$B_{BLAST} = N_t \log_2(M). \tag{4.1}$$

For example, consider BPSK signalling with 4 transmit antennas, then four bits can be transmitted simultaneously by using the BLAST structure. Table 4.1 illustrates the mapping of the BLAST structure for BPSK signalling with 4 transmit antennas.

All possible transmit signal vectors for a given configuration compose the input signal space. The cardinality of the input signal space of BLAST MIMO transmit structure is given by

$$\left| A_{\mathbf{x}_{BLAST}} \right| = M^{N_t}. \tag{4.2}$$

Table 4.1: Mapping table of the BLAST structure for BPSK signalling with 4 transmit antennas

Input Bits	Transmit Signal Vector
0 0 0 0	$\mathbf{x} = \frac{1}{\sqrt{4}} [\ 1 \quad 1 \quad 1 \quad 1\ ]^T$
0 0 0 1	$\mathbf{x} = \frac{1}{\sqrt{4}} [\ 1 \quad 1 \quad 1 \quad -1\ ]^T$
0 0 1 0	$\mathbf{x} = \frac{1}{\sqrt{4}} [\ 1 \quad 1 \quad -1 \quad 1\ ]^T$
0 0 1 1	$\mathbf{x} = \frac{1}{\sqrt{4}} [\ 1 \quad 1 \quad -1 \quad -1\ ]^T$
0 1 0 0	$\mathbf{x} = \frac{1}{\sqrt{4}} [\ 1 \quad -1 \quad 1 \quad 1\ ]^T$
0 1 0 1	$\mathbf{x} = \frac{1}{\sqrt{4}} [\ 1 \quad -1 \quad 1 \quad -1\ ]^T$
0 1 1 0	$\mathbf{x} = \frac{1}{\sqrt{4}} [\ 1 \quad -1 \quad -1 \quad 1\ ]^T$
0 1 1 1	$\mathbf{x} = \frac{1}{\sqrt{4}} [\ 1 \quad -1 \quad -1 \quad -1\ ]^T$
1 0 0 0	$\mathbf{x} = \frac{1}{\sqrt{4}} [\ -1 \quad 1 \quad 1 \quad 1\ ]^T$
1 0 0 1	$\mathbf{x} = \frac{1}{\sqrt{4}} [\ -1 \quad 1 \quad 1 \quad -1\ ]^T$
1 0 1 0	$\mathbf{x} = \frac{1}{\sqrt{4}} [\ -1 \quad 1 \quad -1 \quad 1\ ]^T$
1 0 1 1	$\mathbf{x} = \frac{1}{\sqrt{4}} [\ -1 \quad 1 \quad -1 \quad -1\ ]^T$
1 1 0 0	$\mathbf{x} = \frac{1}{\sqrt{4}} [\ -1 \quad -1 \quad 1 \quad 1\ ]^T$
1 1 0 1	$\mathbf{x} = \frac{1}{\sqrt{4}} [\ -1 \quad -1 \quad 1 \quad -1\ ]^T$
1 1 1 0	$\mathbf{x} = \frac{1}{\sqrt{4}} [\ -1 \quad -1 \quad -1 \quad 1\ ]^T$
1 1 1 1	$\mathbf{x} = \frac{1}{\sqrt{4}} [\ -1 \quad -1 \quad -1 \quad -1\ ]^T$

The discrete time equivalent of the received signal for a flat fading channel is

$$\mathbf{y} = \mathbf{H}\mathbf{x} + \mathbf{w}$$

$$\begin{bmatrix} y_1 \\ y_2 \\ \vdots \\ y_{Nr} \end{bmatrix} = \begin{bmatrix} h_{1,1} & h_{1,2} & .... & h_{1,Nt} \\ h_{2,1} & h_{2,2} & .... & h_{2,Nt} \\ \vdots & \vdots & & \vdots \\ h_{Nr,1} & h_{Nr,2} & .... & h_{Nr,Nt} \end{bmatrix} \begin{bmatrix} x_1 \\ x_2 \\ \vdots \\ x_{Nt} \end{bmatrix} + \begin{bmatrix} w_1 \\ w_2 \\ \vdots \\ w_{Nr} \end{bmatrix} \tag{4.3}$$

where **H** is an $N_r x N_t$ matrix. The parameter $h_{i,m}$ represents the flat fading channel path gain between the m^{th} transmit antenna and the i^{th} receive antenna. The transmit signal **x** is an N_tx1

vector where and x_m represents the transmitted symbol from m^{th} transmit antenna. The power launched by each transmit antenna is proportional to $1/N_t$ so that the total radiated power is constant and independent of N_t. The additive white Gaussian noise **w** and the received signal **y** are N_rx1 vectors where w_i represents the noise symbol on the i^{th} receive antenna and y_i represents the received symbol from the i^{th} receive antenna respectively.

In the BLAST MIMO transmission structure, all transmit antennas operate simultaneously on the same frequency as explained. This causes interchannel interference (ICI) of transmitted sequences at the receiver [4]. In the receiver, computationally complex detection algorithms are needed to overcome the ICI problem.

Since all transmitting antennas are operating simultaneously, multiple radio frequency (RF) chains are needed and inter-antenna synchronization (IAS) must be provided [8]. Both of these requirements increase the hardware complexity.

For operation of BLAST techniques, the number of transmit antennas must be less than or equal to the number of receive antennas [4]. This cause difficulties especially for mobile handsets due to their limited physical size.

Due to these difficulties an alternative MIMO technique to increase spectral efficiency is proposed in [5,6,7,8] which is called Spatial Modulation.

4.3 Spatial Modulation

Spatial Modulation (SM) combines digital modulation and multiple-antenna transmission to increase spectral efficiency of wireless communication systems [5,6,7,8]. In Spatial Modulation only one antenna is active for transmission at a time in contrast to the classical Multiple Input Multiple Output (MIMO) techniques like BLAST structure which is performing spatial multiplexing.

In Spatial Modulation, the basic principle is modulating the symbol with not only phase or amplitude of the carrier but also with selection of the antenna for transmission of the carrier. The location of the activated antenna in spatial domain is used as an information source for transmission of the data and thus spectral efficiency is increased.

The transmitter structure of spatial modulation is shown in Figure 4.6.

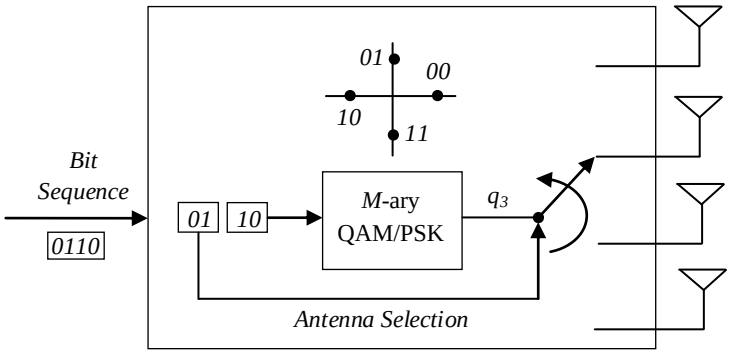

Figure 4.6: Transmitter structure of Spatial Modulation

The number of bits that are mapped into transmit signal vector **x** is given by

$$B_{SM} = \log_2\left(N_t\right) + \log_2\left(M\right) \tag{4.4}$$

where first $\log_2(N_t)$ bits choose the antenna that transmits the signal and last $\log_2(M)$ bits are mapped according to the spatial constellation point.

For example, consider QPSK signalling with 4 transmit antennas, then four bits can be transmitted simultaneously by using spatial modulation. Table 4.2 illustrates the mapping of spatial modulation for QPSK signalling with 4 transmit antennas.

The cardinality of the input signal space of spatial modulation is given by

$$\left|A_{\mathbf{x}_{SM}}\right| = N_t M. \tag{4.5}$$

In spatial modulation, only one antenna remains active during transmission

$$\mathbf{x} = \begin{bmatrix} 0 \\ \vdots \\ s \\ \vdots \\ 0 \end{bmatrix}. \tag{4.6}$$

Table 4.2: Mapping table of the spatial modulation for QPSK signalling with 4 transmit antennas

Input Bits	**Transmit Signal Vector**
0 0 0 0	$\mathbf{x} = [\ 1 \quad 0 \quad 0 \quad 0\ ]^T$
0 0 0 1	$\mathbf{x} = [\ j \quad 0 \quad 0 \quad 0\ ]^T$
0 0 1 0	$\mathbf{x} = [\ -1 \quad 0 \quad 0 \quad 0\ ]^T$
0 0 1 1	$\mathbf{x} = [\ -j \quad 0 \quad 0 \quad 0\ ]^T$
0 1 0 0	$\mathbf{x} = [\ 0 \quad 1 \quad 0 \quad 0\ ]^T$
0 1 0 1	$\mathbf{x} = [\ 0 \quad j \quad 0 \quad 0\ ]^T$
0 1 1 0	$\mathbf{x} = [\ 0 \quad -1 \quad 0 \quad 0\ ]^T$
0 1 1 1	$\mathbf{x} = [\ 0 \quad -j \quad 0 \quad 0\ ]^T$
1 0 0 0	$\mathbf{x} = [\ 0 \quad 0 \quad 1 \quad 0\ ]^T$
1 0 0 1	$\mathbf{x} = [\ 0 \quad 0 \quad j \quad 0\ ]^T$
1 0 1 0	$\mathbf{x} = [\ 0 \quad 0 \quad -1 \quad 0\ ]^T$
1 0 1 1	$\mathbf{x} = [\ 0 \quad 0 \quad -j \quad 0\ ]^T$
1 1 0 0	$\mathbf{x} = [\ 0 \quad 0 \quad 0 \quad 1\ ]^T$
1 1 0 1	$\mathbf{x} = [\ 0 \quad 0 \quad 0 \quad j\ ]^T$
1 1 1 0	$\mathbf{x} = [\ 0 \quad 0 \quad 0 \quad -1\ ]^T$
1 1 1 1	$\mathbf{x} = [\ 0 \quad 0 \quad 0 \quad -j\ ]^T$

Hence, only one of the x_m in the transmit signal vector **x** is nonzero, where m represents the activated antenna and s is a symbol drawn from the M-ary constellation

$$m \in \{1, 2, ..., N_t\}, \tag{4.7}$$

$$s \in \{q_1, q_2, ..., q_M\}. \tag{4.8}$$

The signal is transmitted over an N_rxN_t wireless channel **H**. **H** can be written as a set of vectors where each vector corresponds to the channel path gains between transmit antenna m and receive antennas as follows:

$$\mathbf{H} = \begin{bmatrix} h_{1,1} & h_{1,2} & .... & h_{1,N_t} \\ h_{2,1} & h_{2,2} & .... & h_{2,N_t} \\ \vdots & \vdots & & \vdots \\ h_{N_r,1} & h_{N_r,2} & .... & h_{N_r,N_t} \end{bmatrix}$$

$$= \begin{bmatrix} \mathbf{h}_1 & \mathbf{h}_2 & .... & \mathbf{h}_{N_t} \end{bmatrix} \tag{4.9}$$

where

$$\mathbf{h}_m = \begin{bmatrix} h_{1,m} \\ h_{2,m} \\ \vdots \\ h_{N_r,m} \end{bmatrix}. \tag{4.10}$$

When s is transmitted from the m^{th} transmit antenna, the received signal vector given in (4.3) can be simplified as

$$\begin{aligned} \mathbf{y} &= \mathbf{H}\mathbf{x} + \mathbf{w} \\ &= \mathbf{h}_m s + \mathbf{w}. \end{aligned} \tag{4.11}$$

Since only one antenna is active during the transmission of the symbol, the problem of interchannel interference is inherently avoided so complexity of detection algorithms are drastically reduced [5,6,7,8]. This is seen as the most important contribution of spatial modulation.

There is also no need for interantenna synchronization at the transmitter and only one RF chain[1] is used at the transmitter side which reduces the hardware complexity [5,6,7,8].

As explained earlier, for operation of BLAST techniques, the number of transmit antennas must be less than or equal to the number of receive antennas but only a single receive antenna is needed to perform spatial modulation [5,6,7,8]. These benefits put forward spatial modulation especially for scenarios like downlink communication from base stations to mobile handsets.

Besides these benefits SM has some limitations also. When compared to BLAST, SM can offer only a logarithmic increase in spectral efficiency with the number of transmit antennas. This might limit SM to achieve very high spectral efficiencies for practical numbers of antennas at the transmitter.

Since the spectral efficiency increases by the logarithm of the number of transmit antennas, the number of transmit antennas is usually chosen as a power of two.

[1] Only a single RF chain may not be sufficient when band-limitation of the transmitted signal is considered.

4.4 Multiple Active Spatial Modulation

The idea of using multiple active transmit antennas with spatial modulation is considered first in [27] and this technique called as Generalised Spatial Modulation (GSM). GSM transmits the same symbol over the active antennas and uses a set of active antenna combinations as an information source to increase spectral efficiency. The advantage of GSM is that the number of transmit antennas can be freely chosen instead of being power of two.

The idea of combining GSM with spatial multiplexing is considered in [9,10,11]. In this structure, the set of active antenna combinations is used an information source and each active antenna transmits different data streams. By doing that, spatial multiplexing is implemented on activated antennas and also spatial constellation points are used to convey information. This is indeed a hybrid of spatial modulation and spatial multiplexing. The transmitter structure of multiple active spatial modulation is shown in Figure 4.7.

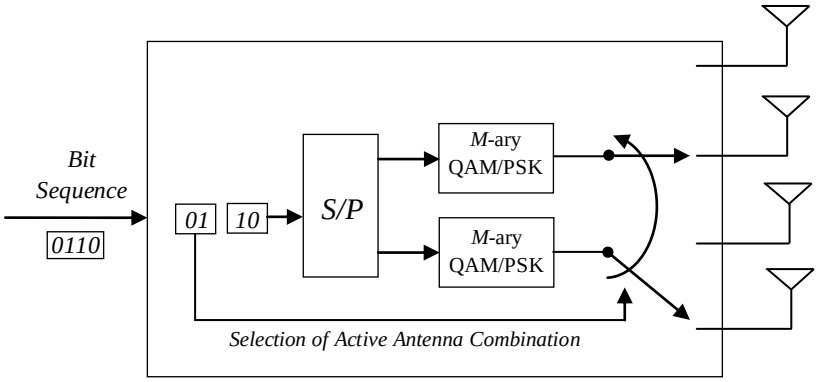

Figure 4.7: Transmitter structure of Multiple Active Spatial Modulation

The number of bits that are mapped into transmit signal vector **x** is given by

$$B_{SM} = \log_2(N_c) + N_a \log_2(M) \tag{4.12}$$

where first $\log_2(N_c)$ bits are mapped according to spatial constellation point which is a set of activated antenna combinations. The last $N_a\log_2(M)$ bits are demultiplexed into N_a substreams. Each substream independently modulated according to same M-ary QAM/PSK constellation and transmitted simultaneously from the activated transmit antennas.

N_c denotes the number of combinations of the active antennas. As told earlier, the number of transmit antennas chosen as power of two in spatial modulation. A similar limitation is valid for number of active antenna combinations in multiple active spatial modulation. For a given configuration, all possible combinations can be larger than a number which is power of two.

Let N_c' denotes the number of all possible combinations which is equal to

$$N_c' = \binom{N_t}{N_a} = \left(\frac{N_t!}{(N_a)!(N_t - N_a)!} \right), \tag{4.13}$$

Then N_c is chosen as

$$N_c = 2^{\lfloor \log_2(N_c') \rfloor}. \tag{4.14}$$

For example, consider BPSK signalling with 4 transmit antennas, then four bits can be transmitted simultaneously by using multiple active spatial modulation. Table 4.3 illustrates the mapping of multiple active spatial modulation for BPSK signalling with 4 transmit antennas.

The number of elements of the input signal space of the multiple active spatial modulation is given by

$$\left| A_{\mathbf{x}_{MA-SM}} \right| = N_c M^{N_a}. \tag{4.15}$$

In multiple active spatial modulation, the antennas $a_1, a_2, \ldots, a_{Na}$ remain active during transmission and hence, only N_a symbols in transmit signal vector is nonzero

$$\mathbf{x} = \begin{bmatrix} 0 & 0 & .. & s_1 & .... & s_{N_a} & .. & 0 & 0 \end{bmatrix}^{\mathrm{T}} \tag{4.16}$$

where $s_1, s_2, \ldots, s_{Na}$ are symbols drawn from the M-ary constellation

$$a_1, a_2, \ldots, a_{Na} \in \{1, 2, ..., N_t\}, \tag{4.17}$$

$$s_1, s_2, \ldots, s_{Na} \in \{q_1, q_2, ..., q_M\}. \tag{4.18}$$

Table 4.3: Mapping table of the multiple active spatial modulation for BPSK signalling with 4 transmit antennas

Input Bits	Transmit Signal Vector
0 0 0 0	$\mathbf{x} = \frac{1}{\sqrt{2}} [\ 1 \quad 0 \quad 1 \quad 0\ ]^T$
0 0 0 1	$\mathbf{x} = \frac{1}{\sqrt{2}} [\ 1 \quad 0 \quad -1 \quad 0\ ]^T$
0 0 1 0	$\mathbf{x} = \frac{1}{\sqrt{2}} [\ -1 \quad 0 \quad 1 \quad 0\ ]^T$
0 0 1 1	$\mathbf{x} = \frac{1}{\sqrt{2}} [\ -1 \quad 0 \quad -1 \quad 0\ ]^T$
0 1 0 0	$\mathbf{x} = \frac{1}{\sqrt{2}} [\ 0 \quad 1 \quad 0 \quad 1\ ]^T$
0 1 0 1	$\mathbf{x} = \frac{1}{\sqrt{2}} [\ 0 \quad 1 \quad 0 \quad -1\ ]^T$
0 1 1 0	$\mathbf{x} = \frac{1}{\sqrt{2}} [\ 0 \quad -1 \quad 0 \quad 1\ ]^T$
0 1 1 1	$\mathbf{x} = \frac{1}{\sqrt{2}} [\ 0 \quad -1 \quad 0 \quad -1\ ]^T$
1 0 0 0	$\mathbf{x} = \frac{1}{\sqrt{2}} [\ 1 \quad 0 \quad 0 \quad 1\ ]^T$
1 0 0 1	$\mathbf{x} = \frac{1}{\sqrt{2}} [\ 1 \quad 0 \quad 0 \quad -1\ ]^T$
1 0 1 0	$\mathbf{x} = \frac{1}{\sqrt{2}} [\ -1 \quad 0 \quad 0 \quad 1\ ]^T$
1 0 1 1	$\mathbf{x} = \frac{1}{\sqrt{2}} [\ -1 \quad 0 \quad 0 \quad -1\ ]^T$
1 1 0 0	$\mathbf{x} = \frac{1}{\sqrt{2}} [\ 0 \quad 1 \quad 1 \quad 0\ ]^T$
1 1 0 1	$\mathbf{x} = \frac{1}{\sqrt{2}} [\ 0 \quad 1 \quad -1 \quad 0\ ]^T$
1 1 1 0	$\mathbf{x} = \frac{1}{\sqrt{2}} [\ 0 \quad -1 \quad 1 \quad 0\ ]^T$
1 1 1 1	$\mathbf{x} = \frac{1}{\sqrt{2}} [\ 0 \quad -1 \quad -1 \quad 0\ ]^T$

The received signal is given by

$$\mathbf{y} = \mathbf{H}\mathbf{x} + \mathbf{w}$$

$$= \left[\mathbf{h}_{a_1}, \ldots, \mathbf{h}_{a_{N_A}}\right]\left[s_1, \ldots, s_{N_A}\right]^T + \mathbf{w} \tag{4.19}$$

As explained earlier, when compared to BLAST, SM can offer only a logarithmic increase in spectral efficiency with the number of transmit antennas. So for high spectral efficiencies, it is becoming hard for SM to compete with BLAST. In such cases MA-SM still could be a low complexity alternative for BLAST.

4.5 Capacity Analysis

We will consider the capacity of MIMO systems for uniformly distributed input constellations. The capacity of the discrete memoryless channels for the given MIMO systems can be calculated by

$$\begin{aligned} C &= I(\mathbf{x};\mathbf{y}) \\ &= D\big[\, p(\mathbf{x},\mathbf{y}) \,\|\, p(\mathbf{x})\,p(\mathbf{y})\big] \\ &= \sum_{\mathbf{x}\in A_{\mathbf{x}}}\sum_{\mathbf{y}\in A_{\mathbf{y}}} p(\mathbf{x},\mathbf{y})\log_2\left(\frac{p(\mathbf{x},\mathbf{y})}{p(\mathbf{x})\,p(\mathbf{y})}\right) \\ &= E_{p(\mathbf{x},\mathbf{y})}\left[\log_2\left(\frac{p(\mathbf{x},\mathbf{y})}{p(\mathbf{x})\,p(\mathbf{y})}\right)\right] \\ &= E_{p(\mathbf{x},\mathbf{y})}\left[\log_2\left(\frac{p(\mathbf{y}\,|\,\mathbf{x})\,p(\mathbf{x})}{p(\mathbf{x})\,p(\mathbf{y})}\right)\right] \\ &= E_{p(\mathbf{x},\mathbf{y})}\left[\log_2\left(\frac{p(\mathbf{y}\,|\,\mathbf{x})}{p(\mathbf{y})}\right)\right] \end{aligned} \tag{4.20}$$

We can write $p(\mathbf{y})$ as

$$p(\mathbf{y}) = \sum_{\mathbf{x}'\in A_{\mathbf{x}}} p(\mathbf{y}\,|\,\mathbf{x}')\,p(\mathbf{x}') \tag{4.21}$$

where $\mathbf{x}'$ is uniformly selected from the input signal space $A_{\mathbf{x}}$. Let us denote the cardinality of the input signal space $A_{\mathbf{x}}$ with $|A_{\mathbf{x}}|$, then under the assumption of equiprobable input symbols, probability $p(\mathbf{x}')$ is

$$p(\mathbf{x}') = \frac{1}{|A_{\mathbf{x}}|} \tag{4.22}$$

and rewriting the capacity we obtain

$$C = E_{p(\mathbf{x},\mathbf{y})}\left[\log_2\left(\frac{p(\mathbf{y}\,|\,\mathbf{x})}{\frac{1}{|A_{\mathbf{x}}|}\sum_{\mathbf{x}'\in A_{\mathbf{x}}} p(\mathbf{y}\,|\,\mathbf{x}')}\right)\right] \tag{4.23}$$

where probability density functions for the given system model can be written as

$$p(\mathbf{y}\,|\,\mathbf{x}) = \left(\frac{1}{\pi N_0}\right)^{N_R} \exp\left(-\frac{\|\,\mathbf{y}-\mathbf{H}\mathbf{x}\,\|^2}{N_0}\right) \tag{4.24}$$

and

$$p(\mathbf{y}\,|\,\mathbf{x}') = \left(\frac{1}{\pi N_0}\right)^{N_R} \exp\left(-\frac{\|\,\mathbf{y}-\mathbf{H}\mathbf{x}'\,\|^2}{N_0}\right). \tag{4.25}$$

Then the capacity can be written as

$$C = E_{p(\mathbf{x},\mathbf{y})}\left[\log_2\left(\frac{\exp\left(-\frac{\|\,\mathbf{y}-\mathbf{H}\mathbf{x}\,\|^2}{N_0}\right)}{\frac{1}{|A_{\mathbf{x}}|}\sum_{\mathbf{x}'\in A_{\mathbf{x}}} \exp\left(-\frac{\|\,\mathbf{y}-\mathbf{H}\mathbf{x}'\,\|^2}{N_0}\right)}\right)\right] \tag{4.26}$$

The capacity of BLAST, SM and MA-SM can be calculated through the Monte Carlo method by following the same procedure. But each time, we have a different input signal space $A_{\mathbf{x}}$ which is determined by its own transmitter structure.

In the following figures, the capacities of given structures for several configurations are depicted. We perform Monte Carlo simulations for 10^4 channel realizations.

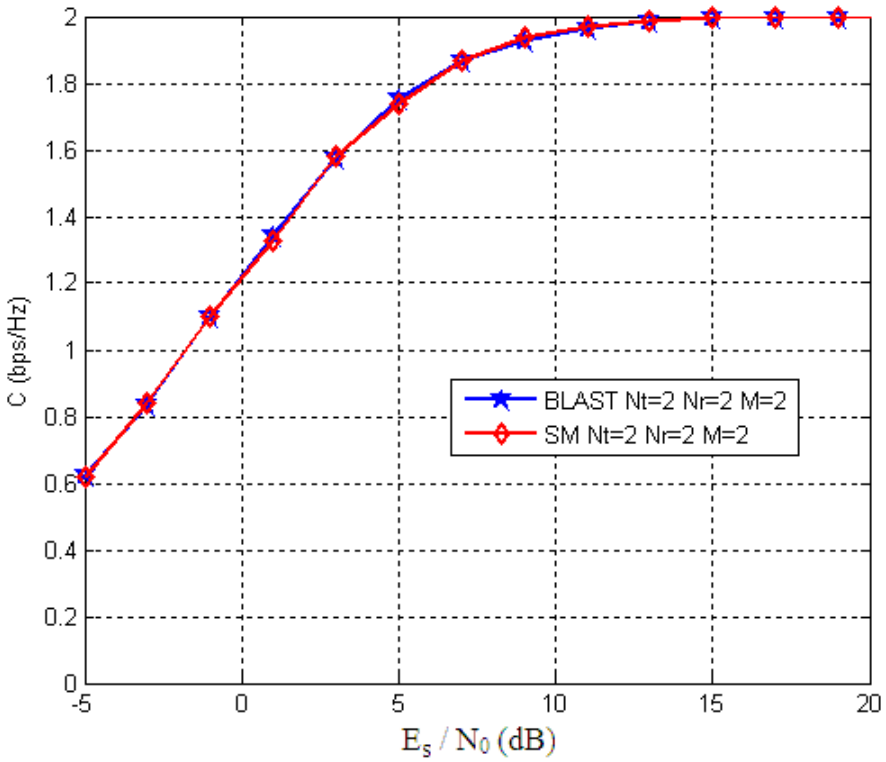

Figure 4.8: Capacity curves for 2bps/Hz with Nt=2 and Nr=2

We can see from Figure 4.8 that SM provides identical performance with the BLAST structure for 2bps/Hz with two transmit and receive antennas.

For the same antenna configuration, the constellation size is enlarged according to the transmission strategy to obtain 4bps/Hz spectral efficiency and the results are depicted in Figure 4.9. SM provides a very close performance to the BLAST structure for this configuration also.

The transmit and receive antenna numbers are increased to four. For this configuration, we can also compare MA-SM with other transmission strategies. For MA-SM with four transmit antennas we choose the active antenna number as two. We can see from Figure 4.10 that SM is significantly superior to both MA-SM and the BLAST structure and MA-SM provides similar performance to the BLAST structure for 4bps/Hz with four transmit and receive antennas.

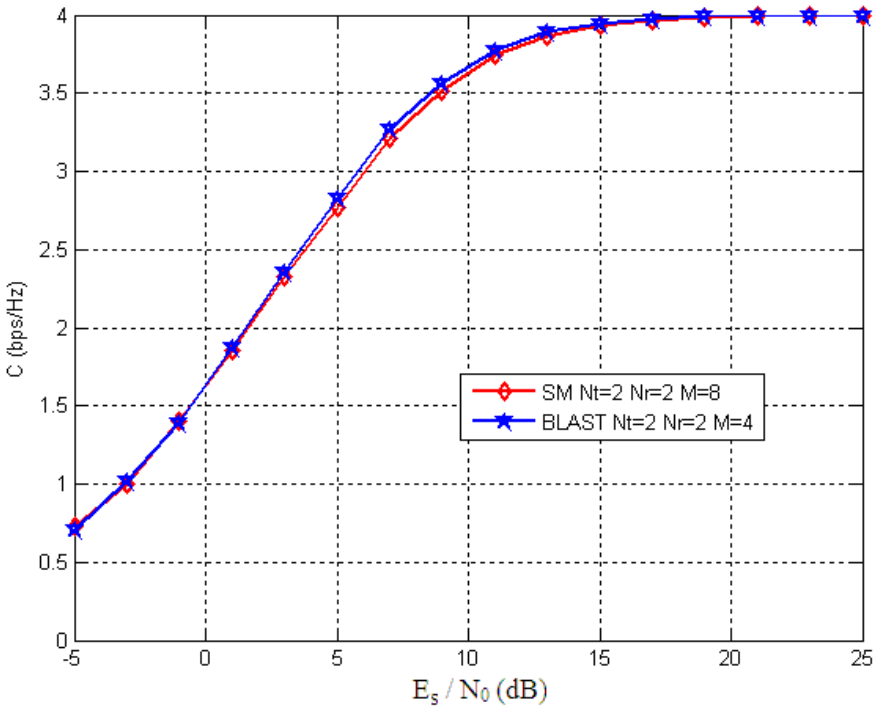

Figure 4.9: Capacity curves for 4bps/Hz with Nt=2 and Nr=2

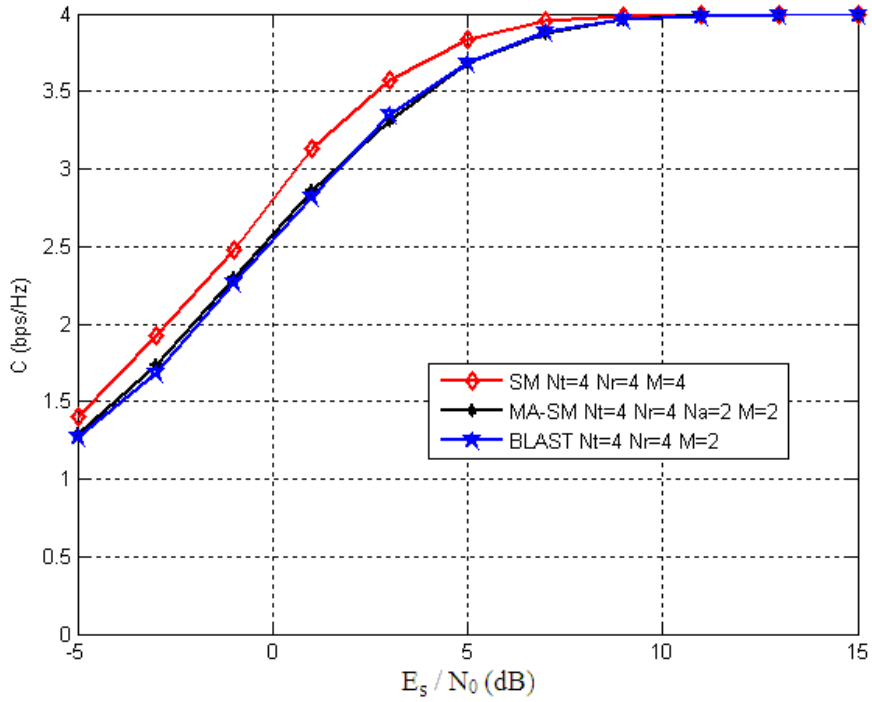

Figure 4.10: Capacity curves for 4bps/Hz with Nt=4 and Nr=4

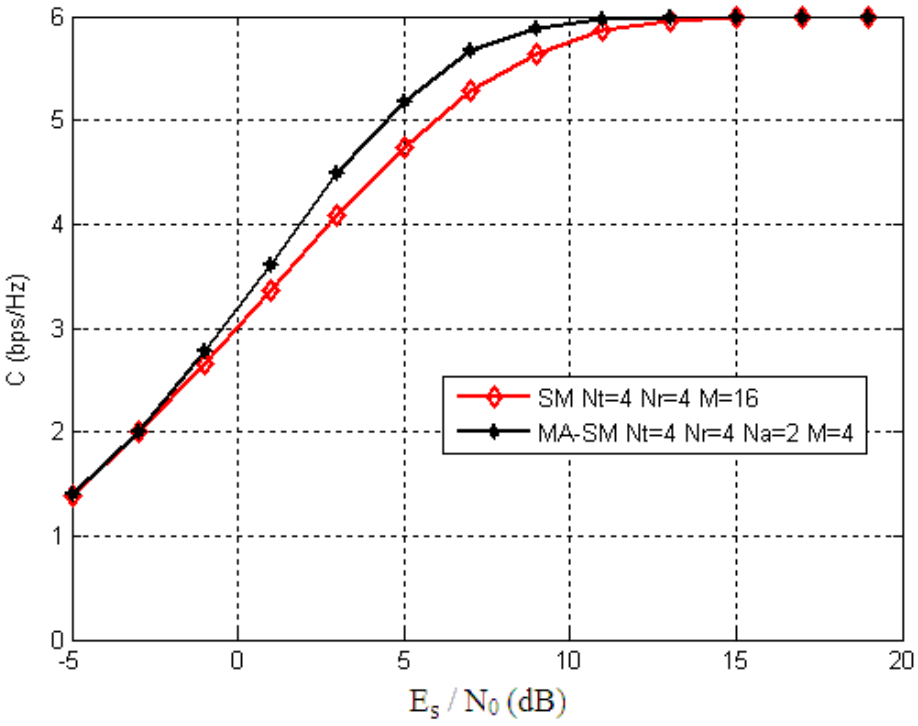

Figure 4.11: Capacity curves for 6bps/Hz with Nt=4 and Nr=4

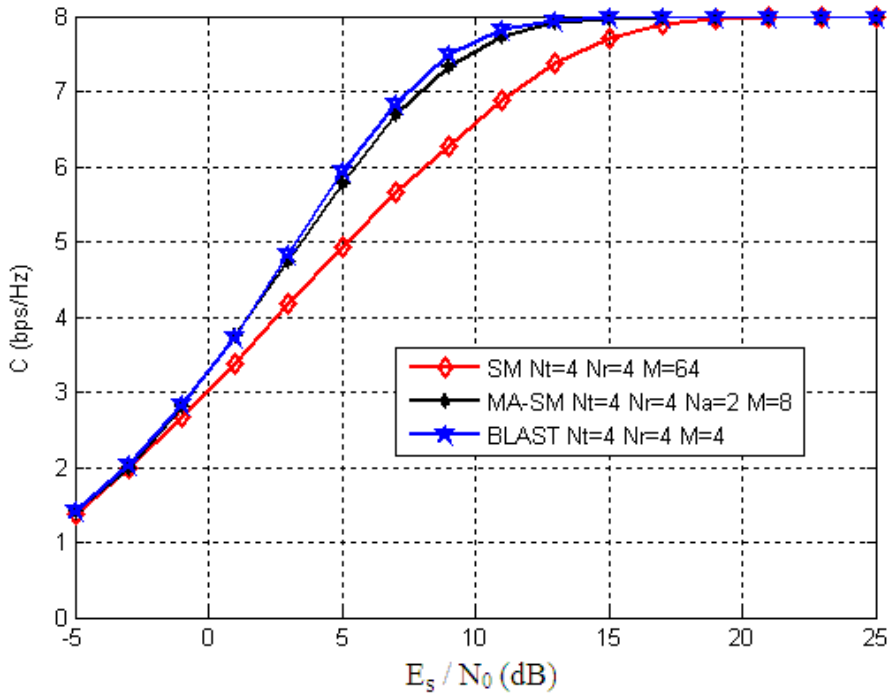

Figure 4.12: Capacity curves for 8bps/Hz with Nt=4 and Nr=4

In Figure 4.11 SM and MA-SM is compared for 6bps/Hz. Since only 4bps/Hz or 8bps/Hz can be obtained by the BLAST structure with four transmit antennas, it is out of comparison here. For this configuration we see that MA –SM is superior to SM which is in contrast to the previous result.

For the same antenna configuration, the constellation sizes are set according to the transmission strategy to obtain 8bps/Hz spectral efficiency and in Figure 4.12 the results are depicted. SM has a poor performance compared to the others but MA-SM yield a close performance to the BLAST structure.

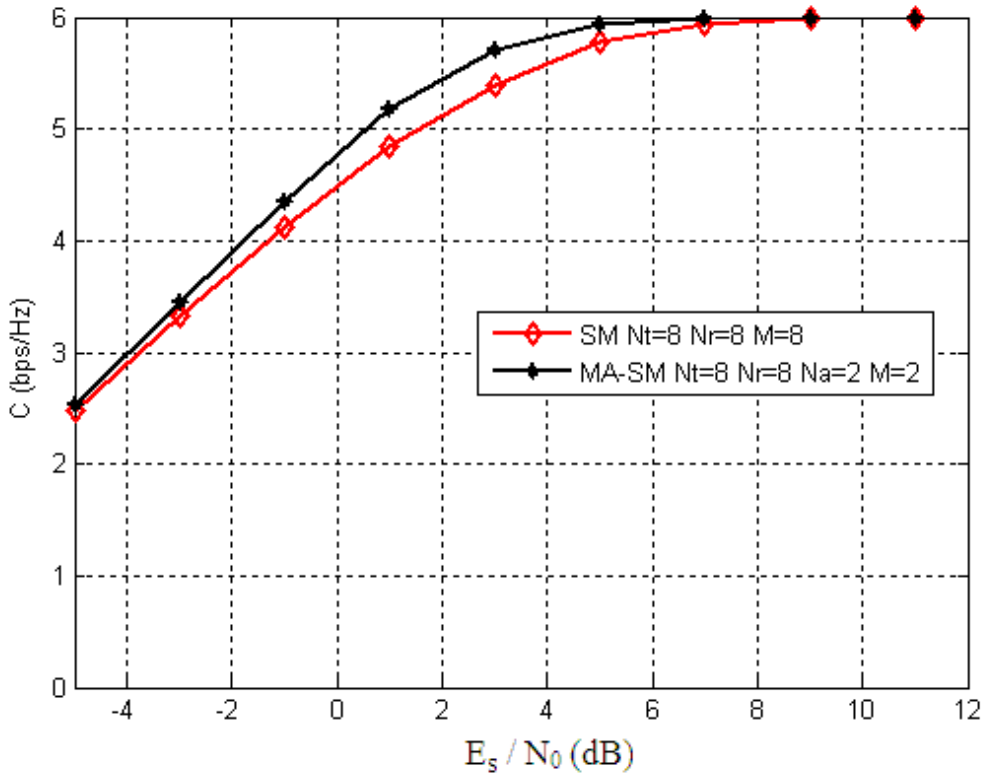

Figure 4.13: Capacity curves for 6bps/Hz with Nt=8 and Nr=8

The transmit and receive antenna numbers are increased to eight. For MA-SM, the number of active antennas is still two. Since the BLAST structure can not provide 6bps/Hz with eight transmit antennas, only SM and MA-SM are compared for this configuration and in Figure 4.13 the results are depicted. MA-SM is again superior to the SM for 6bps/Hz transmission with four transmit and receive antennas.

And finally, the transmission strategies are compared for 8bps/Hz with eight transmit antennas and in Figure 4.14 the results are depicted. MA-SM significantly outperforms SM and the BLAST structure for this configuration and SM shows the poorest performance again.

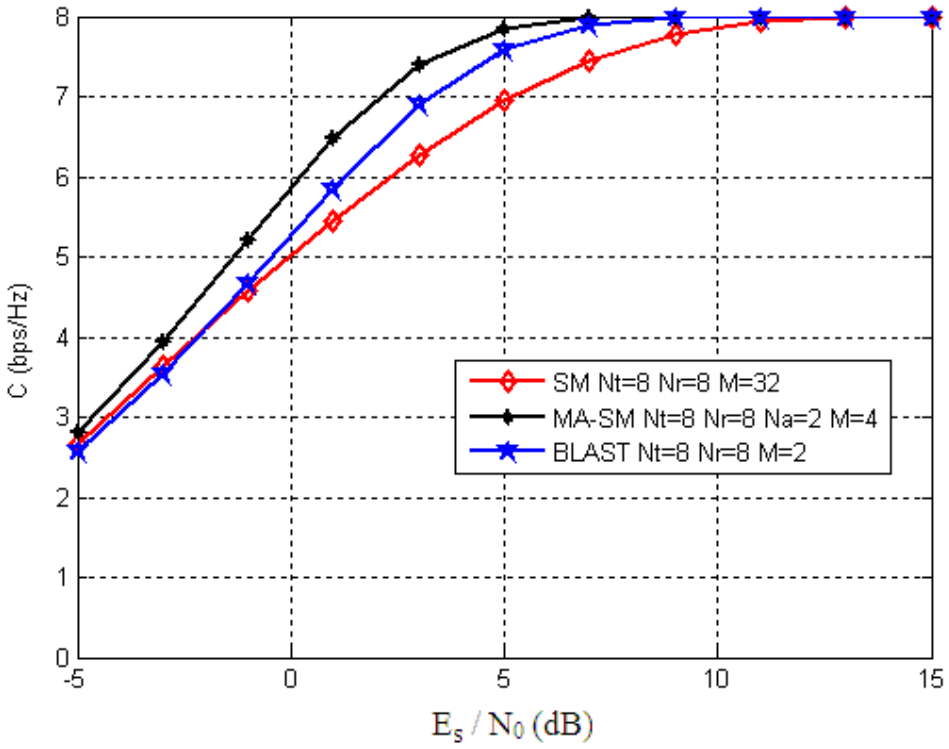

Figure 4.14: Capacity curves for 8bps/Hz with Nt=8 and Nr=8

A remarkable characteristic of SM is observed in simulation results. SM provides an identical performance with the BLAST structure for 2bps/Hz and 4bps/Hz with two transmit and receive antennas and SM outperforms both the BLAST structure and MA-SM for 4bps/Hz with four transmit antennas. However, if we increase spectral efficiency further, SM changes its character completely and its performance deteriorates for high spectral efficiencies.

SM provides a logarithmic increase in spectral efficiency for increasing transmit antennas in contrast to linear increase that the BLAST structure provides. As spectral efficiency increases SM needs to use larger constellation sizes compared to the BLAST structure. For

example, for the configuration of 8bps/Hz transmission with four transmit antennas; SM needs to use 64QAM modulation where the BLAST structure only needs to use QPSK modulation. The performance deterioration due to the high modulation order starts to dominate the performance of SM as spectral efficiency increases. Deterioration in performance of SM for 6bps/Hz and 8bps/Hz transmission can be seen in figures. In these high spectral efficiencies MA-SM still provides a good performance and for 8bps/Hz transmission with eight antennas it is superior to both the BLAST structure and SM.

CHAPTER 5

MIMO SYSTEMS IN MULTIPATH FADING CHANNELS

As explained in previous chapters, there are two main drawbacks of communication systems which are operating with multiple antennas in multipath fading channels. The first problem is intersymbol interference which occurs due to resolvable multipaths between the transmitter and the receiver. The second problem is interchannel interference between multiple antennas since they are operating simultaneously.

In this chapter, a receiver structure for the MIMO systems that are operating in multipath fading channels will be described. The maximum likelihood sequence estimation and the delayed decision feedback sequence estimation techniques derived in Chapter 3 will be expanded for MIMO systems and spatial modulation. The performance of the given multiple antenna techniques in multipath fading channels will be compared.

5.1 MIMO System Model in Multipath Fading

The discrete time transmit signal sequence is given as

$$\mathbf{X} = \left[\mathbf{x}[1] \;\; \mathbf{x}[2] \;\ldots\; \mathbf{x}[N] \right] \tag{5.1}$$

where N denotes the length of the block that is transmitted in each burst. The vector $\mathbf{x}[k]$ denotes the transmitted signal vector at time instant k and it is given as

$$\mathbf{x}[k] = \begin{bmatrix} x_1[k] \\ x_2[k] \\ \vdots \\ x_{N_t}[k] \end{bmatrix} \tag{5.2}$$

where $x_m[k]$ denotes the transmitted symbol from m^{th} transmit antenna at time instant k.

The discrete time channel matrix for the l^{th} tap of ISI channel is given as

$$\mathbf{H}[l]=\begin{bmatrix} h_{1,1}[l] & h_{1,2}[l] & .... & h_{1,N_t}[l] \\ h_{2,1}[l] & h_{2,2}[l] & .... & h_{2,N_t}[l] \\ \vdots & \vdots & & \vdots \\ h_{N_r,1}[l] & h_{N_r,2}[l] & .... & h_{N_r,N_t}[l] \end{bmatrix}. \tag{5.3}$$

The channel path gains are assumed to be quasi-static for a block and independent from block to block. It is also assumed that the length of channel memory is the same for all channels between the transmit and receive antenna pairs. For each path, the channel path gain $h_{i,m}$ is independently and identically distributed according to circularly symmetric complex Gaussian distribution with zero mean and variance $1/L$.

The discrete time received signal sequence is given as

$$\mathbf{Y}=\begin{bmatrix}\mathbf{y}[1] & \mathbf{y}[2] & .... & \mathbf{y}[N]\end{bmatrix} \tag{5.4}$$

where the vector $\mathbf{y}[k]$ denotes the received signal vector at time instant k and it is given as

$$\mathbf{y}[k]=\begin{bmatrix} y_1[k] \\ y_2[k] \\ \vdots \\ y_{N_r}[k] \end{bmatrix} \tag{5.5}$$

with $y_i[k]$ being the received symbol at the i^{th} receive antenna at time instant k. The received signal is written as

$$\mathbf{y}[k]=\sum_{l=0}^{L-1}\mathbf{H}[l]\mathbf{x}[k-l]+\mathbf{w}[k]. \tag{5.6}$$

The time inversed Hermitian (complex conjugate transpose) of the channel matrix is the matched filter for that channel matrix. The output of the matched filter provides sufficient statistics for estimation of the sequence and it is given as

$$\mathbf{z}[n]=\sum_{k=1}^{N}\mathbf{H}^{\mathrm{H}}[k-n]\mathbf{y}[k] \tag{5.7}$$

or equivalently it can be written as

$$\mathbf{z}[n] = \sum_{l=-(L-1)}^{(L-1)} \mathbf{G}[l]\mathbf{x}[n-l] + \mathbf{u}[n] \tag{5.8}$$

where **G** denotes the autocorrelation of the channel matrix and given as

$$\mathbf{G}[l] = \sum_{k=0}^{(L-1)} \mathbf{H}^{\mathrm{H}}[k-l]\mathbf{H}[k] \tag{5.9}$$

and **u**[*n*] denotes the correlated noise samples at the output of the matched filter and has an autocorrelation function of the form

$$E\{\mathbf{u}[n]\mathbf{u}^{\mathrm{H}}[n-l]\} = N_0\mathbf{G}[l]. \tag{5.10}$$

5.2 Optimal Receiver Structure

Maximum likelihood sequence estimation based on the Ungerboeck observation model is the optimal receiver structure [15,16]. The Viterbi algorithm provides an efficient method without loss of optimality [22]. The transmit signal vector **x**[*n*] is chosen from the input signal space $A_{\mathbf{x}}$ with cardinality $|A_{\mathbf{x}}|$, then the number of possible states is $|A_{\mathbf{x}}|^{L-1}$. For each state there are $|A_{\mathbf{x}}|$ possible transitions which means that there are $|A_{\mathbf{x}}|^{L}$ possible transitions in total at a time epoch *n*.

Sequences at a state are directly compared according to their metrics and the sequence with the largest sum will be chosen as the surviving branch for that state and the other branches should be discarded. Since there are $|A_{\mathbf{x}}|^{L-1}$ possible states at time *n*, there will be $|A_{\mathbf{x}}|^{L-1}$ survivors which we have to track. Running this algorithm for each state, the path with the best metric should be picked at the end.

The branch metric for maximum likelihood sequence estimation based on Ungerboeck formulation can be written as

$$BM_n = \mathrm{Re}\left\{\mathbf{x}^{\mathrm{H}}[n]\left[2\mathbf{z}[n] - \mathbf{G}[0]\mathbf{x}[n] - 2\sum_{l=1}^{L-1}\mathbf{G}[l]\mathbf{x}[n-l]\right]\right\}. \tag{5.11}$$

5.2.1 The Computational Complexity of the Optimal Receiver Structure

In this section, we analyze the computational complexity of the proposed receiver structure for the given transmission strategies. We define the computational complexity of the receiver structures as the number of multiplication and addition/subtraction of complex numbers required for calculating the branch metrics. The computational complexity of all branch metrics in a time epoch *n* will be calculated and compared.

The branch metric calculation requires input parameters **z**[*n*] and **G**[*l*] but these parameters need to be calculated once for all branches in a trellis section so computation of these input parameters is ignored in measuring the computational complexity of the branch metrics here.

The BLAST structure uses all transmit antennas simultaneously and all dimensions of the channel matrix. The term $G[l]\mathbf{x}[n\text{-}l]$ needs $2N_t^2 - N_t$ operations. Since same calculation is repeated L times, complexity of these calculations becomes $L(2N_t^2 - N_t)$. After calculation of these terms, there are L vectors with dimension N_tx1 that is going to be subtracted from $z[n]$. These subtractions result in $L(N_t)$ operations in total. After the result is obtained it is going to be multiplied with $\mathbf{x}^{\mathrm{H}}[n]$ which has dimension 1xN_t so this calculation needs $2N_t - 1$ operations. The number of operations needed for calculation of a branch metric for the BLAST structure is given as

$$2LN_t^2 + 2N_t - 1. \tag{5.12}$$

The total computational complexity of all branch metrics calculated in a time epoch *n* for the BLAST structure when the Viterbi algorithm is applied for maximum likelihood sequence estimation becomes

$$\delta_{BLAST,MLSE} = \left[M^{N_t} \right]^L \left[2LN_t^2 + 2N_t - 1 \right]. \tag{5.13}$$

In spatial modulation, only one antenna remains active during transmission. Hence, only one of the terms in the transmit signal vector is nonzero. The term $G[l]\mathbf{x}[n\text{-}l]$ needs N_t operations. Since the same calculation is repeated L times, complexity of these calculations becomes $L(N_t)$. After calculation of these terms, there are L vectors with dimension N_tx1 that is going to be subtracted from $z[n]$. These subtractions result in $L(N_t)$ operations in total. After the result is obtained it is going to be multiplied with $\mathbf{x}^{\mathrm{H}}[n]$ and this calculation needs N_t operations. The number of operations needed for calculation of a branch metric for spatial modulation is given as

$$2LN_t + N_t. \tag{5.14}$$

The total computational complexity for spatial modulation at a time epoch *n* when the Viterbi algorithm is applied on the maximum likelihood sequence estimation becomes

$$\delta_{SM,MLSE} = \left[N_t M\right]^L \left[2LN_t + N_t\right]. \tag{5.15}$$

In multiple active spatial modulation, N_a antennas remains active during transmission. Hence, only N_a symbols in transmit signal vector is nonzero. The term $G[l]\mathbf{x}[n-l]$ needs $2N_tN_a - N_t$ operations. Since the same calculation is repeated L times, complexity of these calculations becomes $L(2N_tN_a - N_t)$. After calculation of these terms, there are L vectors with dimension N_tx1 that is going to be subtracted from $z[n]$. These subtractions result in $L(Nt)$ operations in total. After result is obtained it is going to be multiplied with $\mathbf{x}^H[n]$ and this calculation needs $2N_a - 1$ operations. The number of operations needed for calculation of a branch metric for multiple active spatial modulation is given as

$$2LN_tN_a + 2N_a - 1. \tag{5.16}$$

The total computational complexity for multiple antenna spatial modulation at a time epoch *n* when the Viterbi algorithm is applied on the maximum likelihood sequence estimation becomes

$$\delta_{MA-SM,MLSE} = \left[N_c M^{N_a}\right]^L \left[2LN_tN_a + 2N_a - 1\right]. \tag{5.17}$$

Comparison of the total computational complexities for various configurations in 2-tap and 3-tap ISI channel are given in Table 5.1 and 5.2 respectively. It can be seen that spatial modulation has the lowest complexity and the BLAST structure has the highest complexity for all configurations. SM provides reduction up to %85 in computational complexity compared to the BLAST structure according to the configuration. MA-SM also provides reduction up to %75 in computational complexity compared to the BLAST structure according to the configuration.

Table 5.1: Computational complexity of MLSE in a 2-tap ISI channel

Configuration	BLAST	SM	MA-SM
Nt=2 Nr=2 2bps/Hz	304	160	-
Nt=2 Nr=2 4bps/Hz	4,864	2,560	-
Nt=4 Nr=4 4bps/Hz	18,176	5,120	8,960
Nt=4 Nr=4 6bps/Hz	-	81,920	143,360
Nt=4 Nr=4 8bps/Hz	4,653,056	1,310,720	2,293,760
Nt=8 Nr=8 6bps/Hz	-	163,840	274,432
Nt=8 Nr=8 8bps/Hz	17,760,256	2,621,440	4,390,912

Table 5.2: Computational complexity of MLSE in a 3-tap ISI channel

Configuration	BLAST	SM	MA-SM
Nt=2 Nr=2 2bps/Hz	1,728	896	-
Nt=2 Nr=2 4bps/Hz	110,592	57,344	-
Nt=4 Nr=4 4bps/Hz	421,888	114,688	208,896
Nt=4 Nr=4 6bps/Hz	-	7,340,032	13,369,344
Nt=4 Nr=4 8bps/Hz	1,728,100,000	469,762,048	855,638,016
Nt=8 Nr=8 6bps/Hz	-	14,680,064	25,952,256
Nt=8 Nr=8 8bps/Hz	6,694,100,000	939,524,096	1,660,900,000

5.2.2 Simulation Results of the Optimal Receiver Structure

The bit error rate performances of the given multiple antenna transmission techniques with the proposed optimal receiver structure are compared using Monte Carlo simulations. In the simulations, each block to be transmitted in a burst has a length of 500 bits and each simulation was run for a count of 2000 bit errors. In the following figures, the bit error rates for several configurations are depicted.

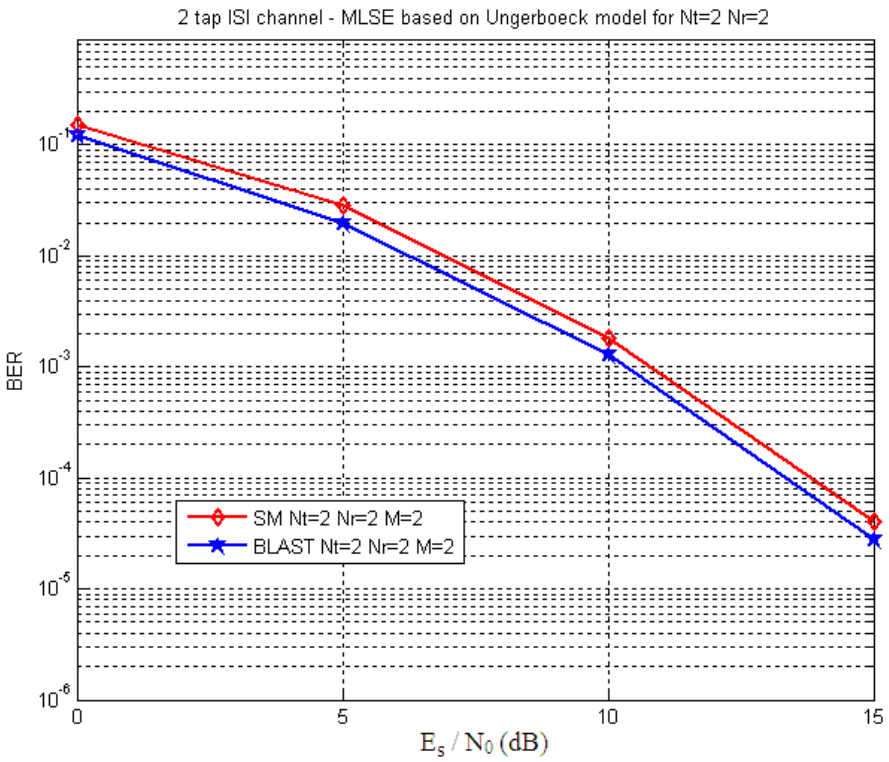

Figure 5.1: MLSE in a 2-tap ISI channel for 2bps/Hz transmission with Nt=2 and Nr=2

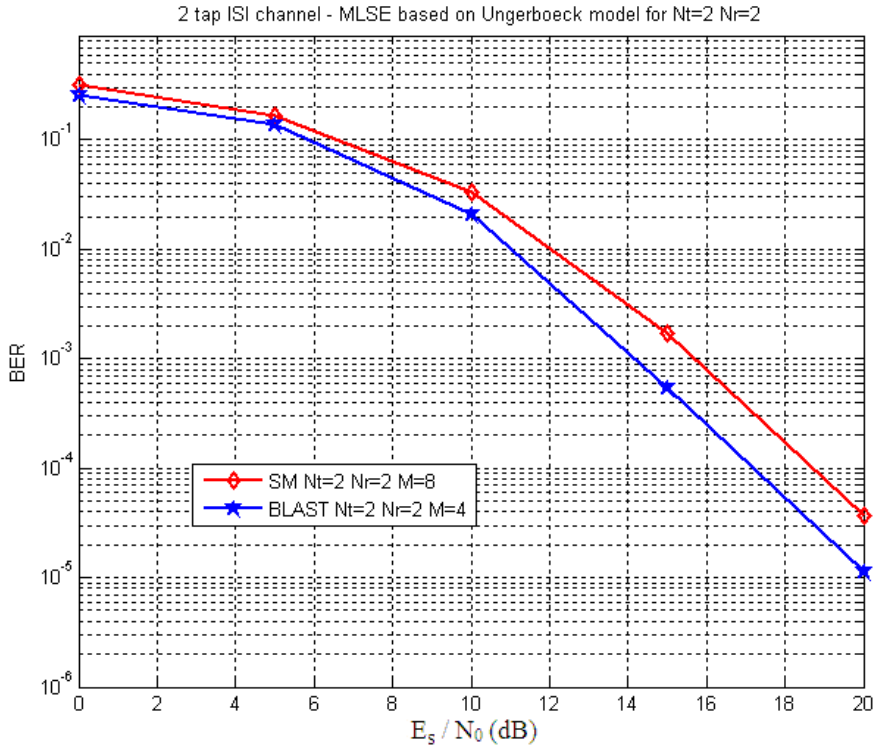

Figure 5.2: MLSE in a 2-tap ISI channel for 4bps/Hz transmission with Nt=2 and Nr=2

The bit error rate results of SM and the BLAST structure for 2bps/Hz and 4bps/Hz transmission with two transmit and receive antennas in 2-tap ISI channel are depicted in Figure 5.1. and 5.2 respectively. For these configurations, SM provides approximately %50 reduction in computational complexity compared to the BLAST structure but SM lose 0.5 dB and 1.5 dB at a bit error rate 10^{-3} compared to the BLAST structure for 2bps/Hz and 4bps/Hz transmission respectively.

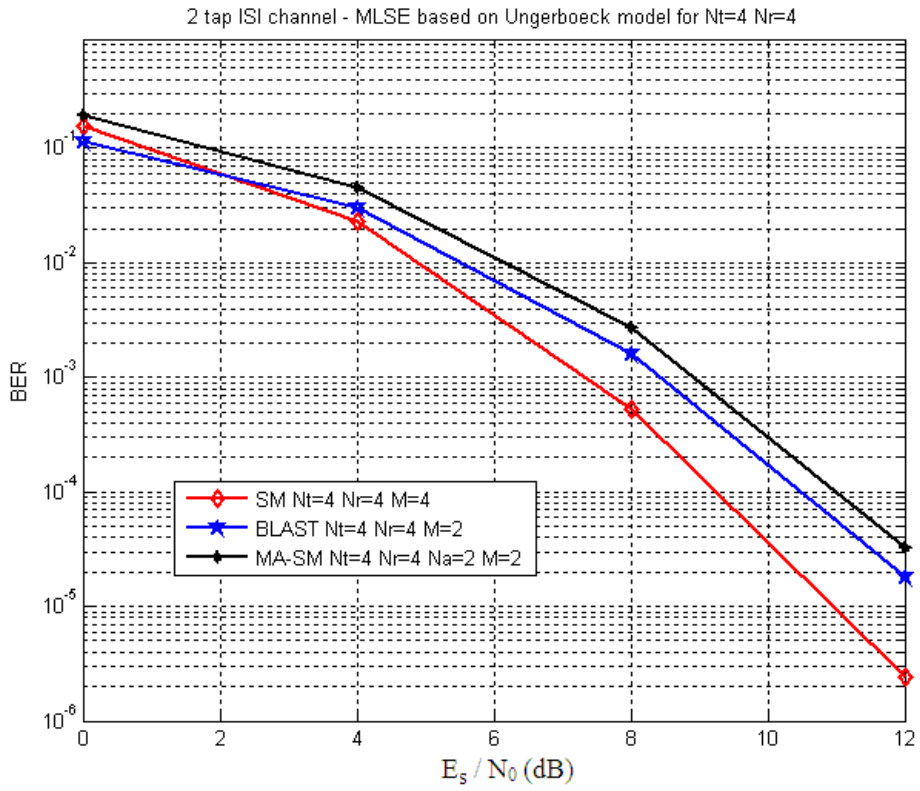

Figure 5.3: MLSE in a 2-tap ISI channel for 4bps/Hz transmission with Nt=4 and Nr=4

The bit error rate results of SM, MA-SM and the BLAST structure for 4bps/Hz transmission with four transmit and receive antennas in 2-tap ISI channel are depicted in Figure 5.3. MA-SM uses only two antennas simultaneously. For this configuration, SM provides approximately %50 and %72 reduction in computational complexity compared to the MA-SM and the BLAST structure and respectively. SM gains 1.0 dB over the BLAST structure and 1.5 dB over the MA-SM at a bit error rate 10^{-3}.

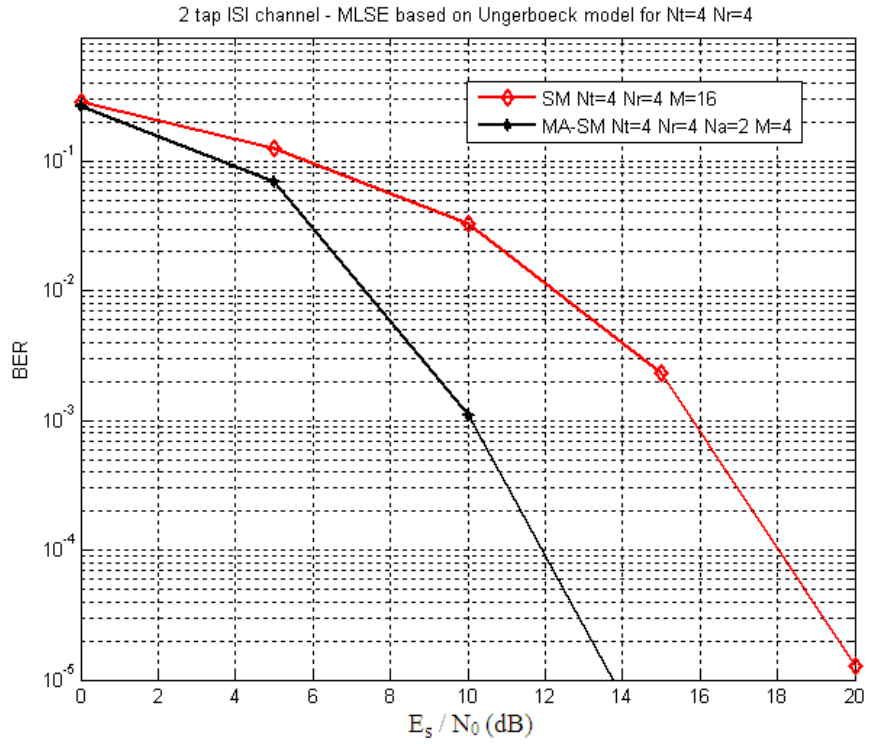

Figure 5.4: MLSE in a 2-tap ISI channel for 6bps/Hz transmission with Nt=4 and Nr=4

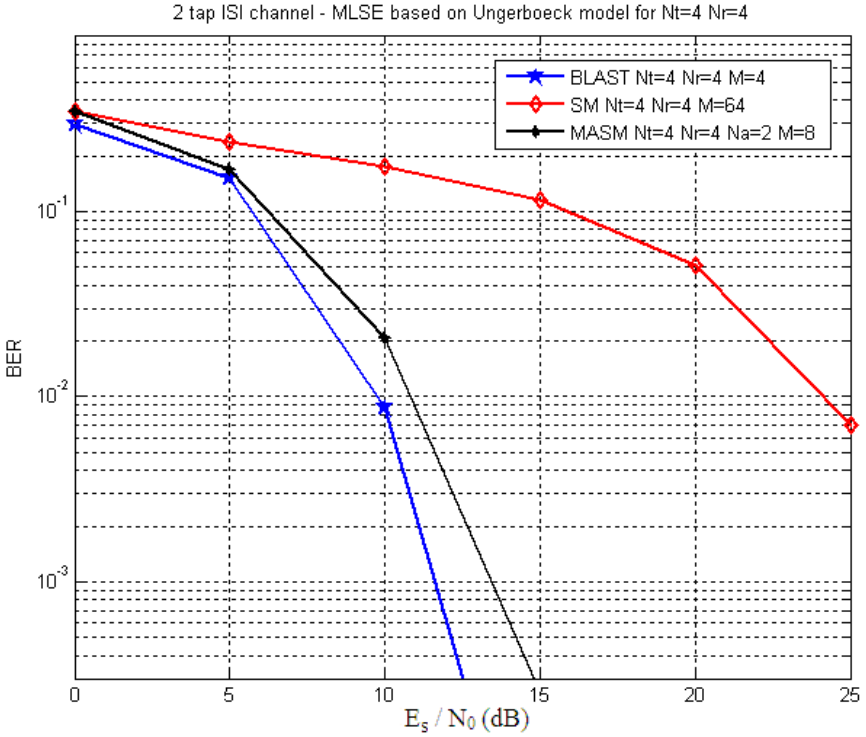

Figure 5.5: MLSE in a 2-tap ISI channel for 8bps/Hz transmission with Nt=4 and Nr=4

The bit error rate results of SM and MA-SM for 6bps/Hz transmission with four transmit and receive antennas in 2-tap ISI channel are depicted in Figure 5.4. Since 6bps/Hz transmission can not be obtained for the BLAST structure with four transmit antennas without coding, it is out of comparison here. For this configuration, it can be seen that SM has a very poor performance and MA-SM is 6.0 dB better than SM at 10^{-3} bit error rate.

The bit error rate results of SM, MA-SM and the BLAST structure for 8bps/Hz transmission with four transmit and receive antennas in 2-tap ISI channel are depicted in Figure 5.5. MA-SM uses only two antennas simultaneously. For this configuration, the BLAST structure is significantly superior to the SM but gain is less than 1.5 dB compared to the MA-SM.

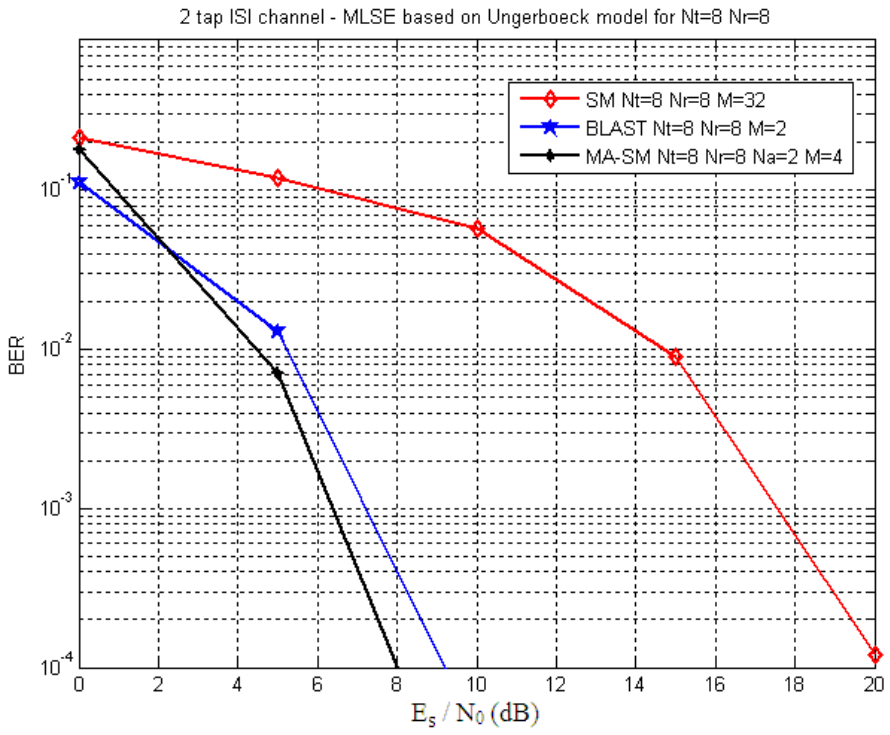

Figure 5.6: MLSE in a 2-tap ISI channel for 8bps/Hz transmission with Nt=8 and Nr=8

The bit error rate results of SM, MA-SM and the BLAST structure for 8bps/Hz transmission with eight transmit and receive antennas in 2-tap ISI channel are depicted in Figure 5.6. MA-SM uses only two antennas simultaneously. For this configuration, MA-SM outperforms the BLAST and SM where SM has a significant performance loss.

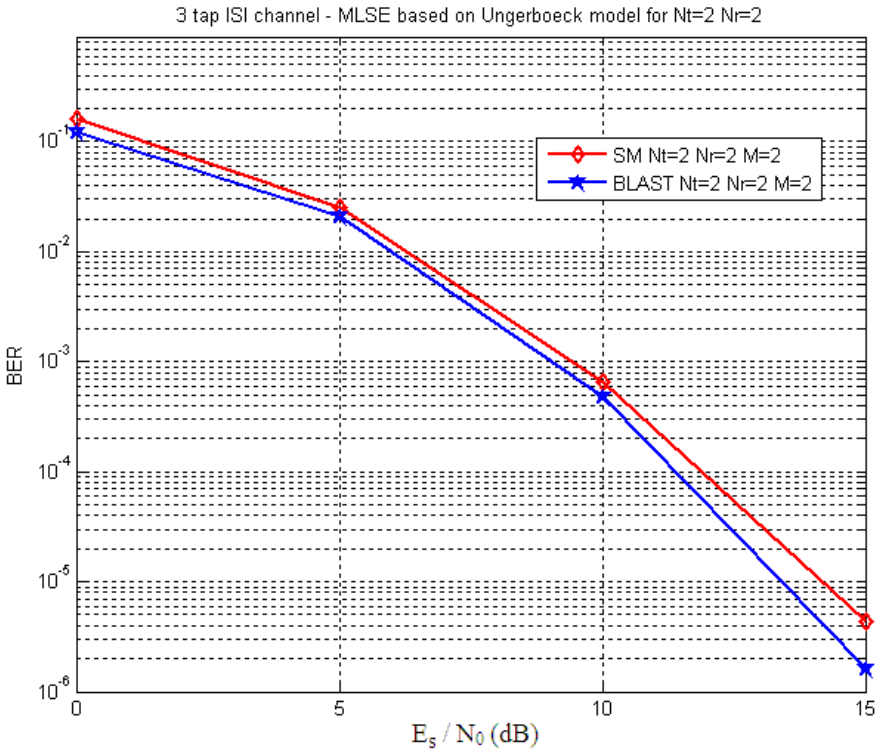

Figure 5.7: MLSE in a 3-tap ISI channel for 2bps/Hz transmission with Nt=2 and Nr=2

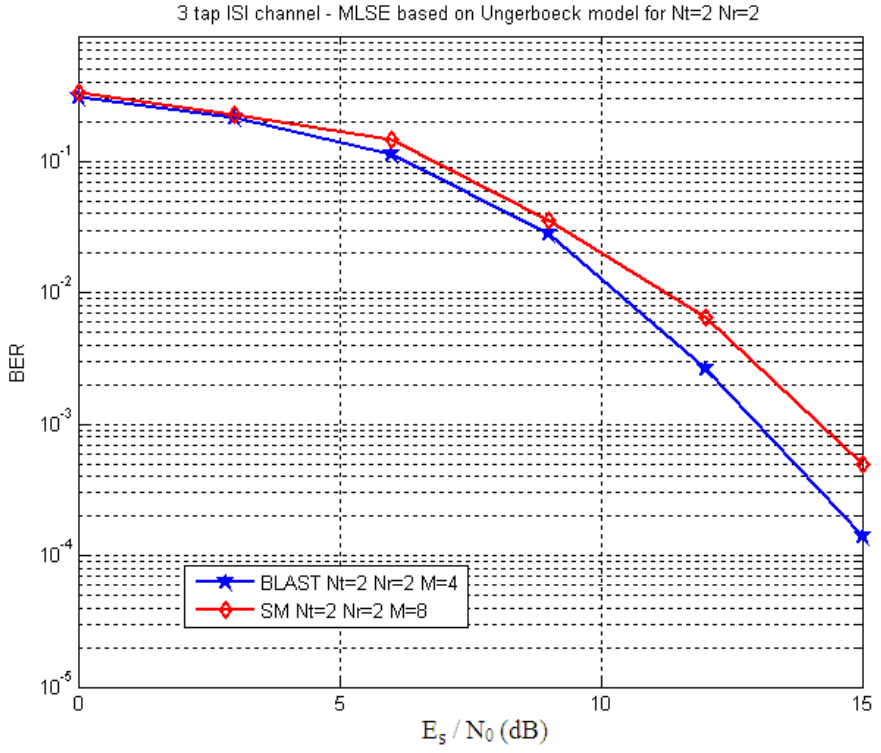

Figure 5.8: MLSE in a 3-tap ISI channel for 4bps/Hz transmission with Nt=2 and Nr=2

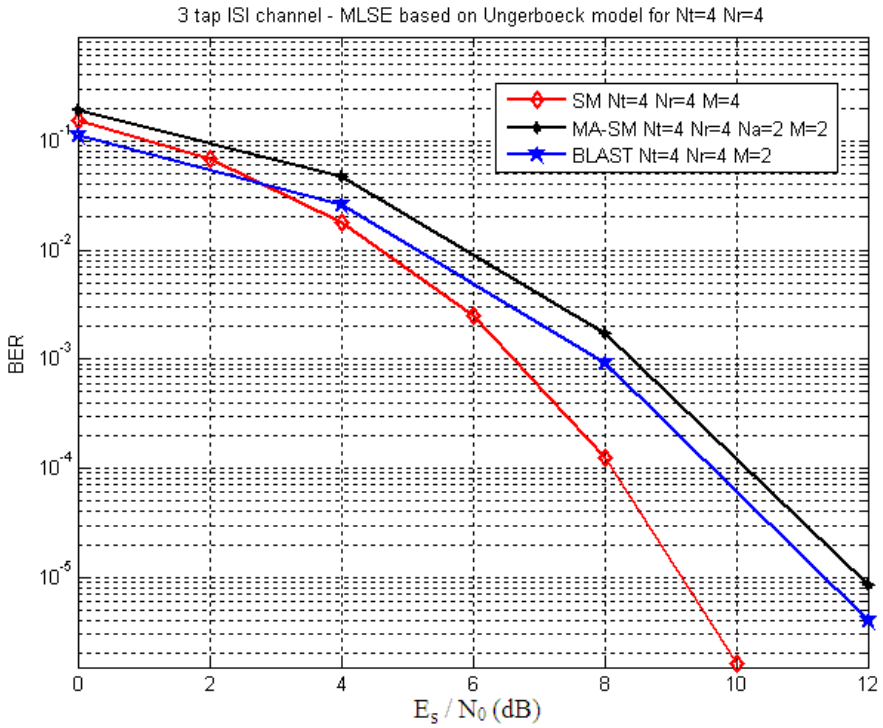

Figure 5.9: MLSE in a 3-tap ISI channel for 4bps/Hz transmission with Nt=4 and Nr=4

The bit error rate results of SM, MA-SM and the BLAST structure for 3-tap ISI channel are given in Figures 5.7-5.9. SM causes 0.4 dB performance loss at 10^{-3} bit error rate for 2bps/Hz transmission and 1.2 dB performance loss at 10^{-3} bit error rate for 4bps/Hz transmission with two transmit and receive antennas. For 4bps/Hz transmission with four transmit and receive antennas, SM gains 1.3dB and 1.8dB compared to the BLAST structure and MA-SM respectively.

5.3 Suboptimal Receiver Structure

Delayed decision feedback sequence estimation is a reduced complexity suboptimal alternative for maximum likelihood sequence estimation [17,18,19]. The channel order J is a control parameter for the trade-off between complexity and performance. States are defined based on past J symbols so the number of states for an input signal space with cardinality $|A_{\mathbf{x}}|$ equals to $|A_{\mathbf{x}}|^J$.

Memory order J is chosen between zero and the length of the channel memory $L-1$ so that we obtain a reduced state trellis. The estimates of the remaining past symbols from $J+1$ to $L-1$ are obtained by tracking the surviving path leading to each state and these estimates of the remaining past symbols are used in calculating the branch metrics.

The branch metric for DDFSE based on the Ungerboeck formulation can be written as

$$BM_n = \mathrm{Re}\left\{\mathbf{x}^{\mathrm{H}}[n]\left[2\mathbf{z}[n]-\mathbf{G}[0]\mathbf{x}[n]-2\sum_{l=1}^{J}\mathbf{G}[l]\mathbf{x}[n-l]-2\sum_{l=J+1}^{L-1}\mathbf{G}[l]\hat{\mathbf{x}}[n-l]\right]\right\}. \quad (5.18)$$

where ($\mathbf{x}[n\text{-}1]$, $\mathbf{x}[n\text{-}2]$,…, $\mathbf{x}[n\text{-}J]$) are considered as the vectors that make up the state in trellis and ($\hat{\mathbf{x}}[n\text{-}J\text{-}1]$, $\hat{\mathbf{x}}[n\text{-}J\text{-}2]$,…, $\hat{\mathbf{x}}[n\text{-}L\text{+}1]$) are considered as feedback of the decisions which are obtained by tracking the surviving path leading to that state.

5.3.1 The Computational Complexity of the Suboptimal Receiver Structure

In delayed decision feedback sequence estimation, only the number of branch metrics to be calculated is different and it is controlled by memory order *J*.

The total computational complexity for the BLAST structure at a time epoch *n* when the Viterbi algorithm is applied on the delayed decision feedback sequence estimation becomes

$$\delta_{BLAST,DDFSE} = \left[M^{N_t}\right]^{J+1}\left[2LN_t^2+2N_t-1\right]. \quad (5.19)$$

The total computational complexity for spatial modulation at a time epoch *n* when the Viterbi algorithm is applied on the delayed decision feedback sequence estimation becomes

$$\delta_{SM,DDFSE} = \left[N_t M\right]^{J+1}\left[2LN_t+N_t\right]. \quad (5.20)$$

The total computational complexity for multiple antenna spatial modulation at a time epoch *n* when the Viterbi algorithm is applied on delayed decision feedback sequence estimation becomes

$$\delta_{MA-SM,DDFSE} = \left[N_c M^{N_a}\right]^{J+1}\left[2LN_tN_a+2N_a-1\right]. \quad (5.21)$$

Comparison of the total computational complexities for various configurations in 3-tap ISI channel with memory order J=1 and 4-tap ISI channel with memory order J=1 and J=2 are given in Table 5.3, 5.4 and 5.5 respectively. It can be seen that spatial modulation has the lowest complexity and the BLAST structure has the highest complexity for all configurations. DDFSE provides reduction more than %75 in total computational complexity compared to the MLSE counterparts.

Table 5.3: Computational complexity of DDFSE in a 3-tap ISI channel with J=1

Configuration	**BLAST**	**SM**	**MA-SM**
Nt=2 Nr=2 2bps/Hz	432	224	-
Nt=2 Nr=2 4bps/Hz	6,912	3,584	-
Nt=4 Nr=4 4bps/Hz	26,368	7,168	13,056
Nt=4 Nr=4 6bps/Hz	-	114.688	208,896
Nt=4 Nr=4 8bps/Hz	6,750,208	1,835,008	3,342,336
Nt=8 Nr=8 6bps/Hz	-	229,376	405,504
Nt=8 Nr=8 8bps/Hz	26,148,864	3,670,016	6,488,064

Table 5.4: Computational complexity of DDFSE in a 4-tap ISI channel with J=1

Configuration	**BLAST**	**SM**	**MA-SM**
Nt=2 Nr=2 2bps/Hz	560	288	-
Nt=2 Nr=2 4bps/Hz	8,960	4,608	-
Nt=4 Nr=4 4bps/Hz	34,560	9,216	17,152
Nt=4 Nr=4 6bps/Hz	-	147,456	274,432
Nt=4 Nr=4 8bps/Hz	8,847,360	2,359,296	4,390,912
Nt=8 Nr=8 6bps/Hz	-	294,912	536,576
Nt=8 Nr=8 8bps/Hz	34,537,472	4,718,592	8,585,216

Table 5.5: Computational complexity of DDFSE in a 4-tap ISI channel with J=2

Configuration	BLAST	SM	MA-SM
Nt=2 Nr=2 2bps/Hz	2,240	1,152	-
Nt=2 Nr=2 4bps/Hz	143,360	73,728	-
Nt=4 Nr=4 4bps/Hz	552,960	147,456	274,432
Nt=4 Nr=4 6bps/Hz	-	9,437,184	17,563,648
Nt=4 Nr=4 8bps/Hz	2,264,900,000	603,979,776	1,124,100,000
Nt=8 Nr=8 6bps/Hz	-	18,874,368	34,340,864
Nt=8 Nr=8 8bps/Hz	8,841,600,000	1,208,000,000	2,197,800,00

5.3.2 Simulation Results of the Suboptimal Receiver Structure

The bit error rate performances of the given multiple antenna transmission techniques with the proposed suboptimal receiver structure are compared using Monte Carlo simulations. In the simulations, each block to be transmitted in a burst has a length of 500 bits and each simulation was run for a count of 2000 bit errors. In the following figures, the comparisons of performances for several configurations are depicted.

The bit error rate results of SM and the BLAST structure for 2bps/Hz and 4bps/Hz transmission with two transmit and receive antennas in 3-tap ISI channel with memory order J=1 are depicted in Figure 5.10 and 5.11 respectively. For these configurations, SM provides performances very close to the BLAST structure but the BLAST structure still outperform SM.

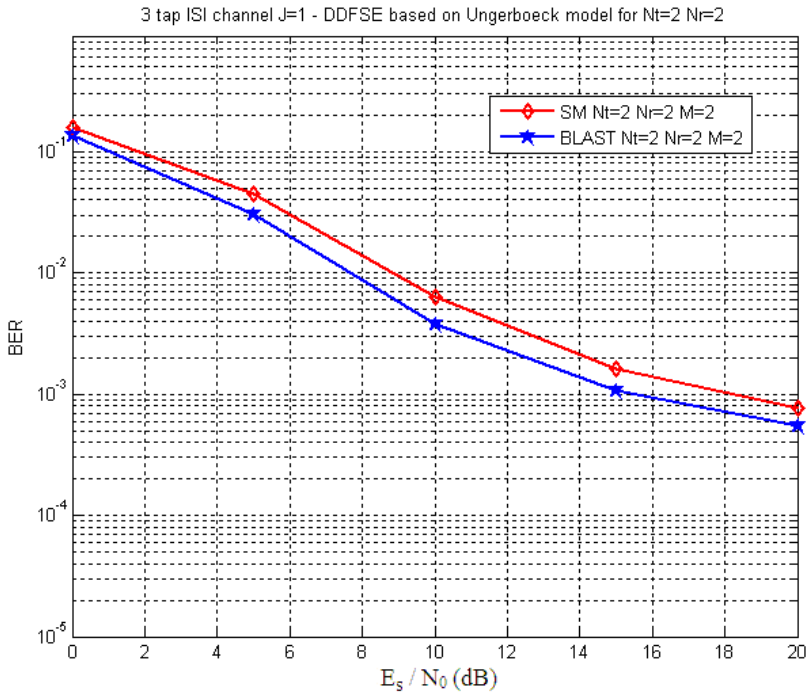

Figure 5.10: DDFSE in a 3-tap ISI channel with *J*=1 for 2bps/Hz transmission with Nt=2 and Nr=2

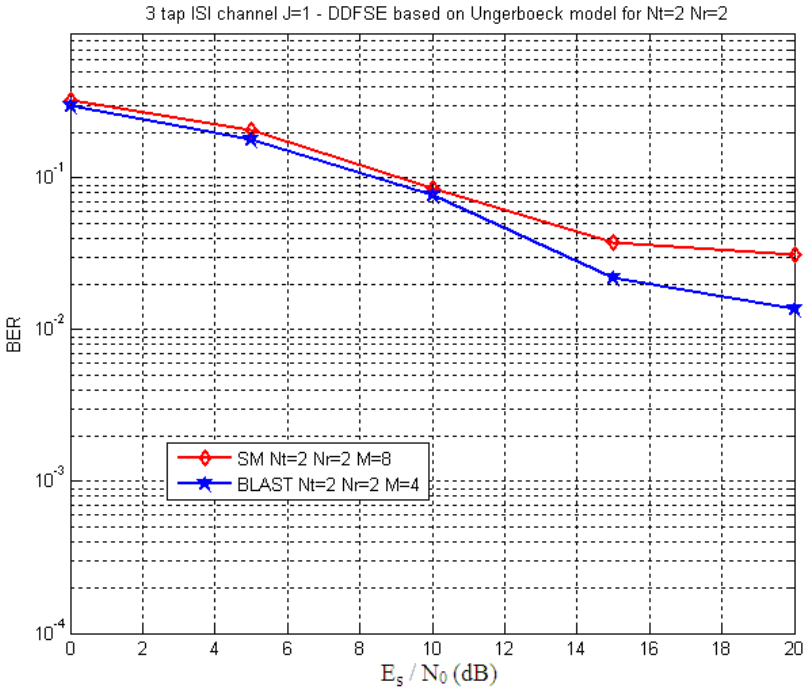

Figure 5.11: DDFSE in a 3-tap ISI channel with *J*=1 for 4bps/Hz transmission with Nt=2 and Nr=2

Figure 5.12 shows the bit error rates results of SM, MA-SM and the BLAST structure for 4bps/Hz transmission with four transmit and receive antennas in 3-tap ISI channel with memory order J=1. For this configuration, SM is 4.0 dB better than the BLAST structure and 5dB better than the MA-SM for 10^{-3} bit error rate.

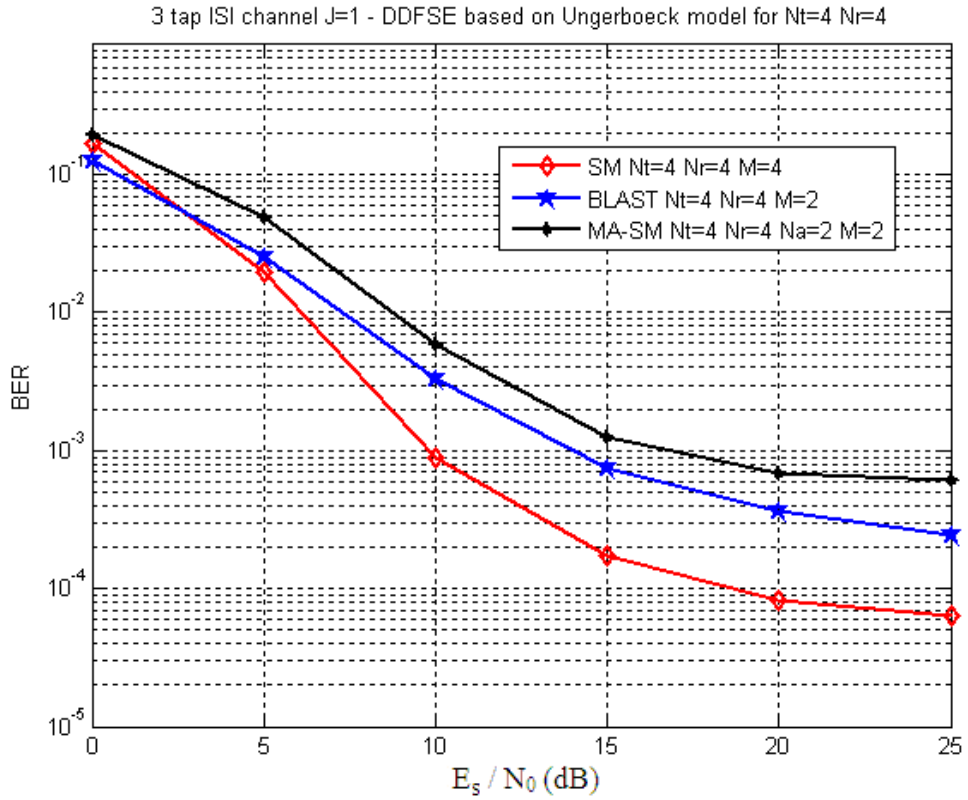

Figure 5.12: DDFSE in a 3-tap ISI channel with J=1 for 4bps/Hz transmission with Nt=4 and Nr=4

Figure 5.13 shows the bit error rates results of SM and MA-SM for 6bps/Hz transmission with four transmit and receive antennas in 3-tap ISI channel with memory order J=1. For this configuration, it can be seen that MA-SM leads to a good performance but SM has a considerable performance loss compared to MA-SM.

Figure 5.14 shows the bit error rates results of SM, MA-SM and the BLAST structure for 8bps/Hz transmission with four transmit and receive antennas in 3-tap ISI channel with memory order J=1. For this configuration, SM yields an unacceptable performance where the BLAST structure and MA-SM provides satisfactory performances.

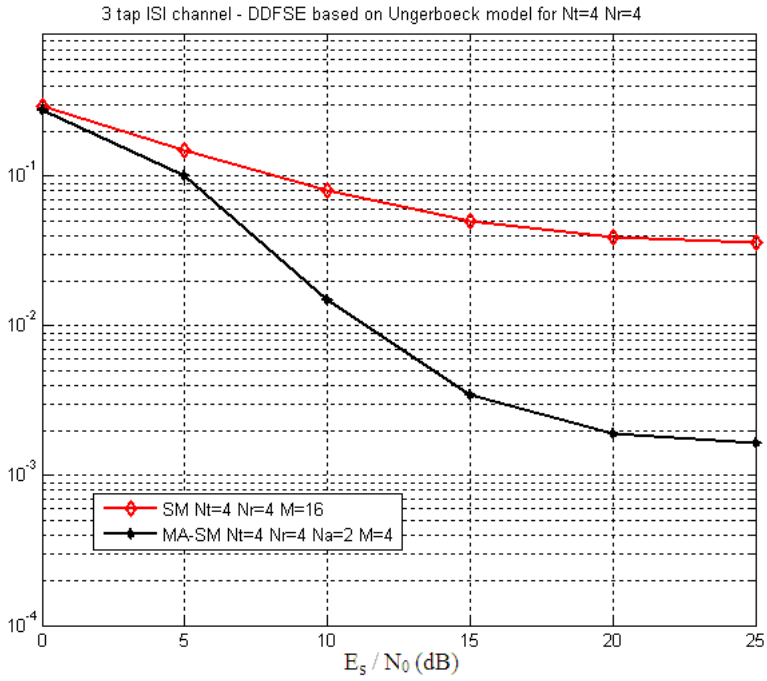

Figure 5.13: DDFSE in a 3-tap ISI channel with *J*=1 for 6bps/Hz transmission with Nt=4 and Nr=4

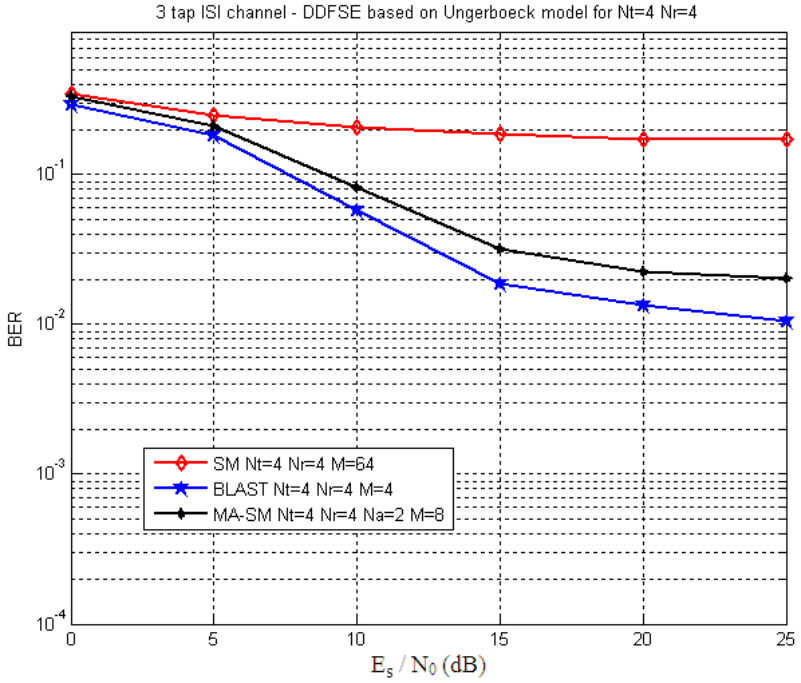

Figure 5.14: DDFSE in a 3-tap ISI channel with *J*=1 for 8bps/Hz transmission with Nt=4 and Nr=4

The bit error rates results for 8bps/Hz transmission with eigth transmit and receive antennas in 3-tap ISI channel with memory order J=1 are depicted in Figure 5.15. SM has the worst performance again where MA-SM is significantly superior to the BLAST structure.

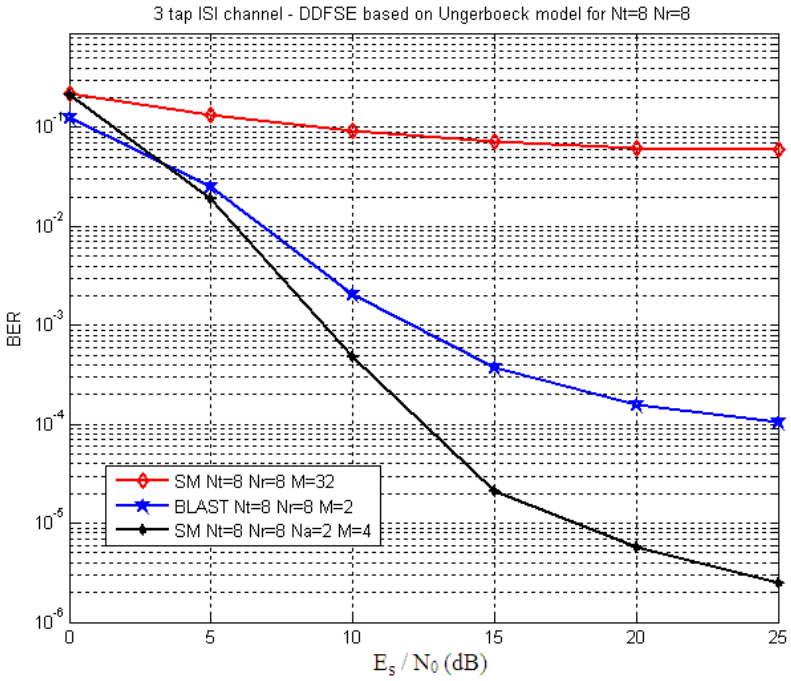

Figure 5.15: DDFSE in a 3-tap ISI channel with J=1 for 8bps/Hz transmission with Nt=8 and Nr=8

The bit error rate results of SM and the BLAST structure for 2bps/Hz and 4bps/Hz transmission with two transmit and receive antennas in 4-tap ISI channel with memory order J=1 are depicted in Figure 5.16 and 5.17 respectively. For these configurations, SM provides performances very close to the BLAST structure but we observe higher bit error rates for both systems since we keep memory order small.

Figure 5.18 shows the bit error rates results of SM, MA-SM and the BLAST structure for 4bps/Hz transmission with four transmit and receive antennas in 4-tap ISI channel with memory order J=1. For this configuration, SM provides a satisfactory performance and outperforms MA-SM and the BLAST structure.

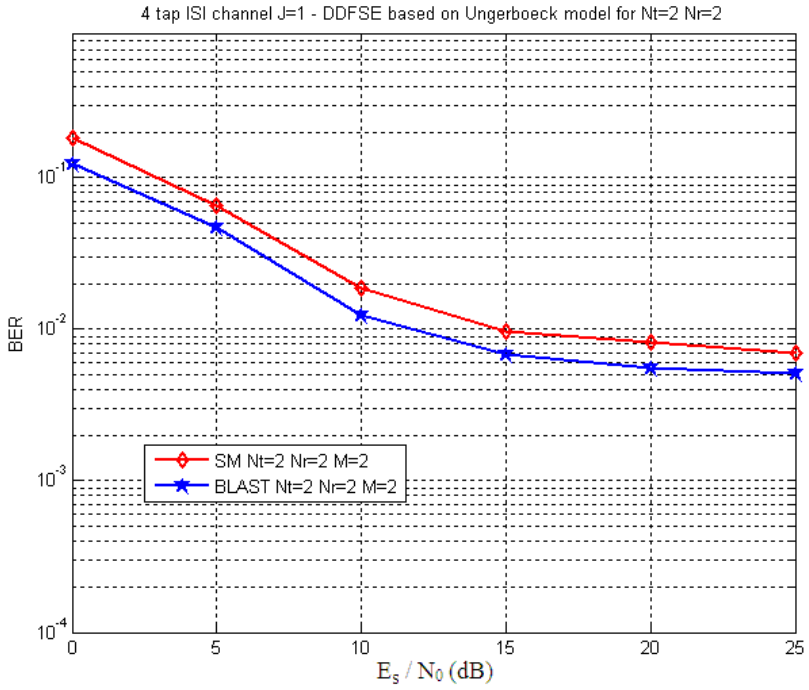

Figure 5.16: DDFSE in a 4-tap ISI channel with *J*=1 for 2bps/Hz transmission with Nt=2 and Nr=2

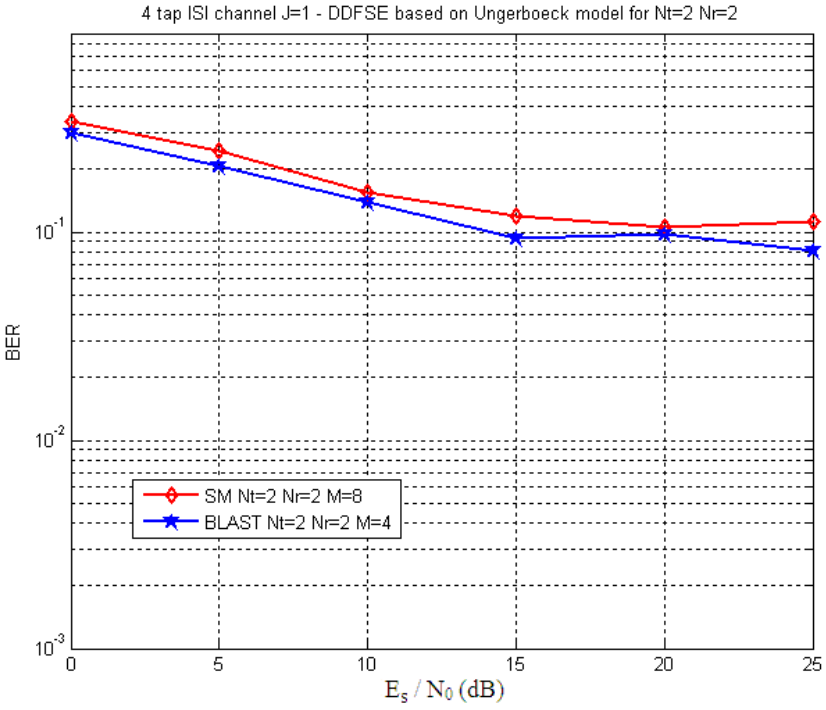

Figure 5.17: DDFSE in a 4-tap ISI channel with *J*=1 for 4bps/Hz transmission with Nt=2 and Nr=2

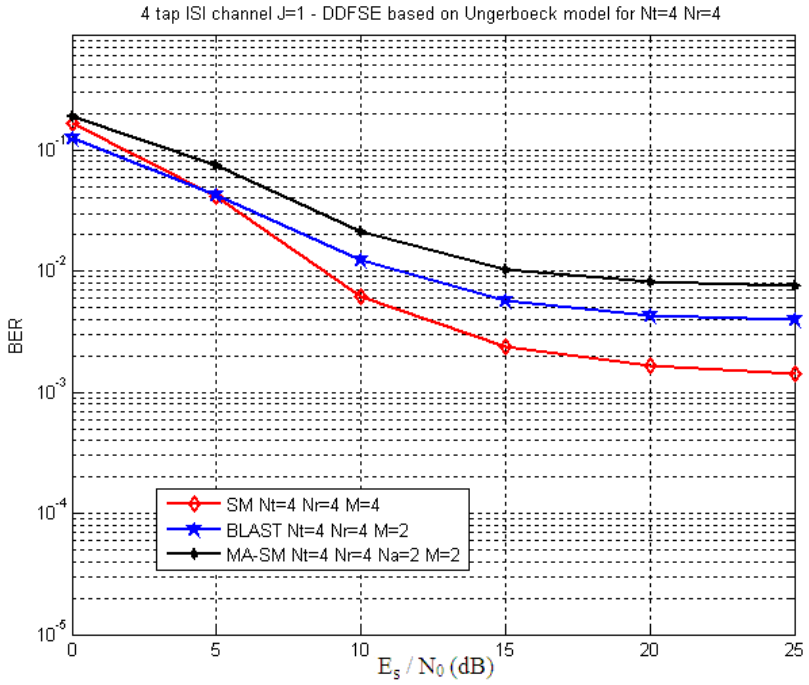

Figure 5.18: DDFSE in a 4-tap ISI channel with *J*=1 for 4bps/Hz transmission with Nt=4 and Nr=4

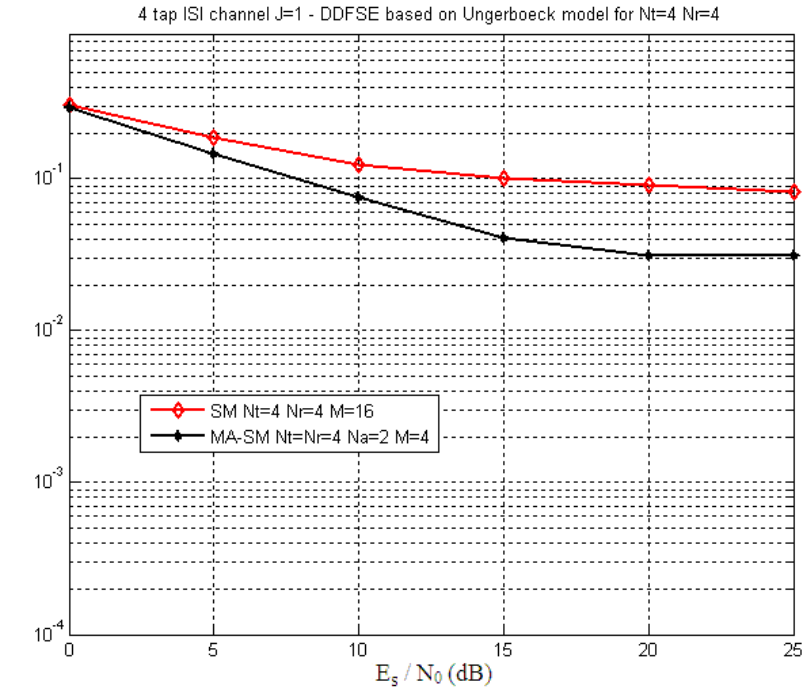

5.19: DDFSE in a 4-tap ISI channel with *J*=1 for 6bps/Hz transmission with Nt=4 and Nr=4

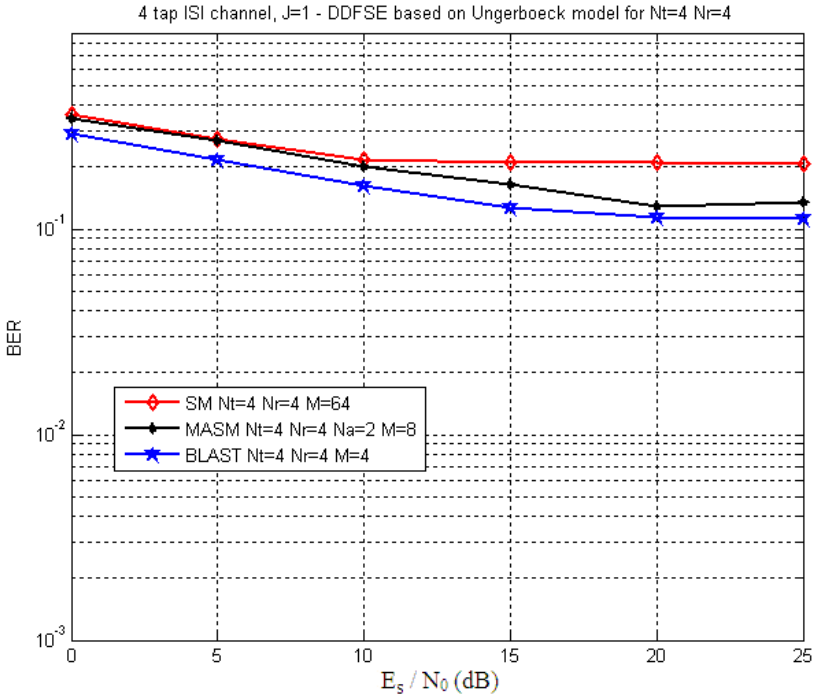

5.20: DDFSE in a 4-tap ISI channel with *J*=1 for 8bps/Hz transmission with Nt=4 and Nr=4

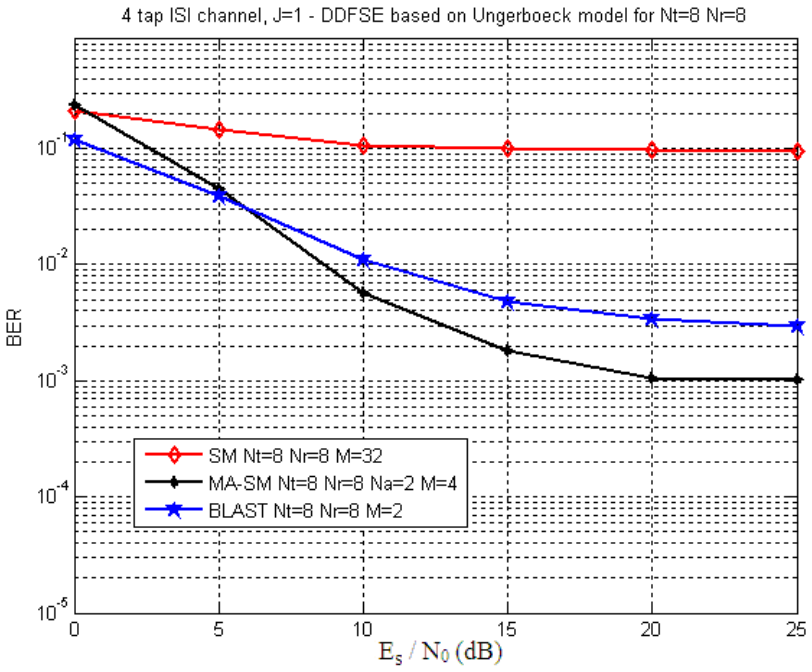

5.21: DDFSE in a 4-tap ISI channel with *J*=1 for 8bps/Hz transmission with Nt=8 and Nr=8

The bit error rate results of SM, MA-SM and the BLAST structure for 6bps/Hz and 8bps/Hz transmission in 4 tap ISI channel with memory order J=1 are depicted in Figures 5.19-5.21. For these configurations, SM yields to an unacceptable where performance of MA-SM and the BLAST structure is still satisfactory.

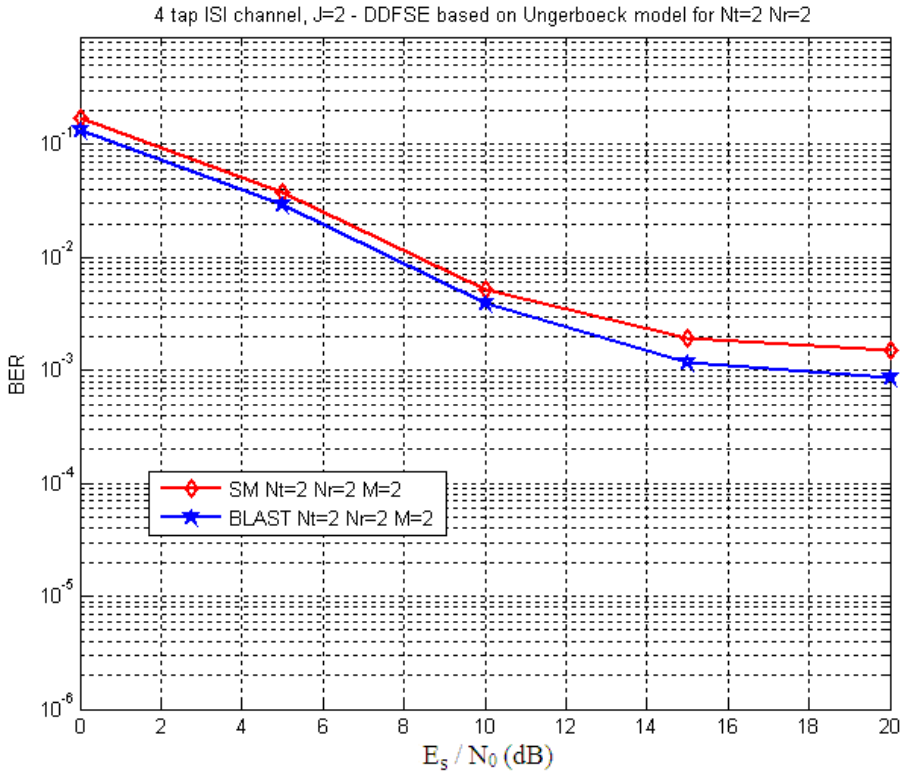

5.22: DDFSE in a 4-tap ISI channel with J=2 for 2bps/Hz transmission with Nt=2 and Nr=2

The bit error rate results of SM, MA-SM and the BLAST structure for 4-tap ISI channel with memory order J=1 are depicted in Figures 5.22-5.24. SM provides close performance to the BLAST structure for 2bps/Hz and 4bps/Hz transmission with two transmit and receive antennas. For 4bps/Hz transmission with four transmit and receive antennas, SM gains 4dB and 5dB compare to the BLAST structure and MA-SM respectively for 10^{-3} bit error rate.

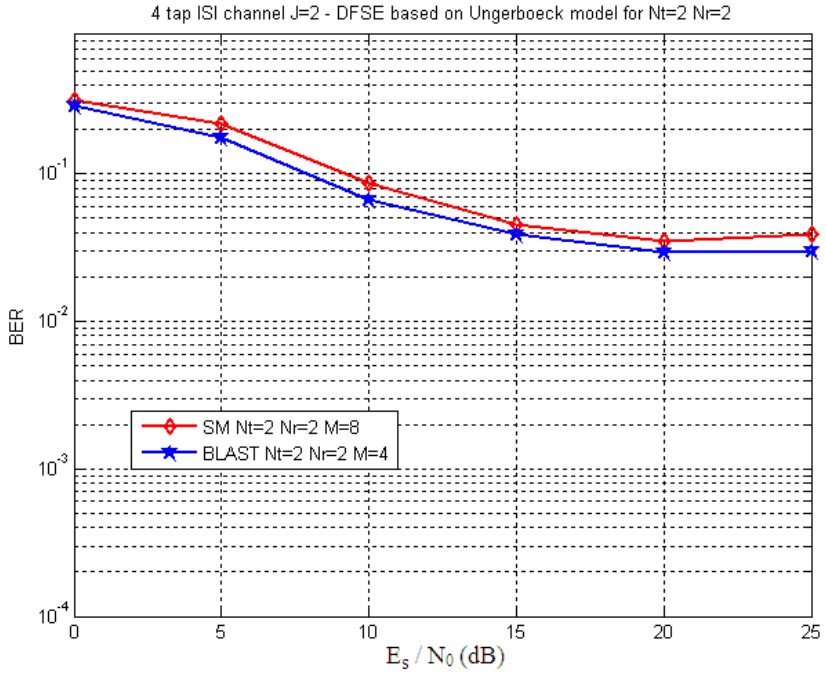

5.23: DDFSE in a 4-tap ISI channel with *J*=2 for 4bps/Hz transmission with Nt=2 and Nr=2

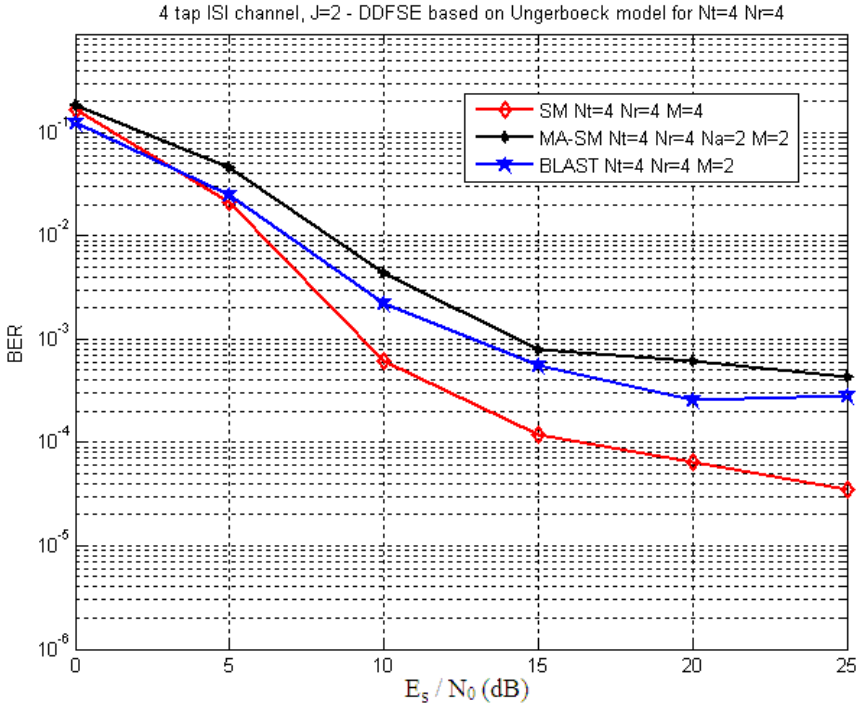

5.24: DDFSE in a 4-tap ISI channel with J=2 for 4bps/Hz transmission with Nt=4 and Nr=4

CHAPTER 6

CONCLUSION

In this thesis, we first studied sequence estimation based on Forney and Ungerboeck observation models for channels with intersymbol interference. Calculation of branch metrics for each observation model is described for both full state trellis search and reduced state trellis search. Forney's formulation for branch metric calculation depends directly on coefficients of channel obtained after whitening filter which means that Forney's metric is sensitive to type and phase of channel which can be considered as a weakness. Ungerboeck's formulation for branch metric calculation depends on output of the matched filter and autocorrelation function of channel which means that Ungerboeck's metric is insensitive to the type and phase of the channel. We compared Forney and Ungerboeck observation models in 2-tap, 3-tap and 4-tap ISI channels using the Monte Carlo simulation method. Both observation models perform identical results for full state maximum likelihood sequence estimation. However, Ungerboeck observation model is superior to Forney's for reduced state delayed decision feedback sequence estimation. Also DDFSE based on the Ungerboeck model eliminates the need to calculate a whitening filter. Due to these benefits, DDFSE based on Ungerboeck model is preferred for the suboptimal case which is of interest in this thesis.

Next, the transmitter structures of spatial multiplexing, spatial modulation and multiple active spatial modulation are given and capacity values of the mentioned MIMO systems for uniformly distributed input constellations are computed and compared using the Monte Carlo simulation method. SM provides an identical performance with the BLAST structure for 2bps/Hz and 4bps/Hz with two transmit and receive antennas and SM outperforms both the BLAST structure and MA-SM for 4bps/Hz with four transmit antennas. However, if we increase the spectral efficiency further, SM changes its character completely and its performance deteriorates for high spectral efficiencies. SM provides a logarithmic increase in spectral efficiency for increasing transmit antennas in contrast to linear increase that the BLAST structure provides. As spectral efficiency increases SM needs to use larger constellation sizes compared to the BLAST structure. The performance deterioration due to the high modulation order starts to dominate the performance of SM as spectral efficiency increases. In high spectral efficiencies MA-SM still provides a good performance and for 8bps/Hz transmission with eight antennas it is superior to both the BLAST structure and SM.

As a next step, the studied multiple antenna techniques are considered in multipath fading channels. First, a receiver structure performing maximum likelihood sequence estimation

based on the Ungerboeck observation model is proposed for the given multiple antenna techniques. Spatial modulation has the smallest complexity and provides reduction up to %85 in computational complexity compared to the BLAST structure according to the configuration. We compared these transmission strategies in 2-tap and 3-tap ISI channels for different spectral efficiencies using the Monte Carlo simulation method. Spatial modulation has a close performance to the BLAST structure for low spectral efficiencies. and provides better performance compared to the others for the scenario of 4bps/Hz transmission with four transmit and receive antennas. Multiple active spatial modulation has a higher complexity compared to spatial modulation but it performs remarkably better in high spectral efficiencies and attain the performance of the BLAST structure with a lower computational complexity.

Finally, delayed decision feedback sequence estimation based on the Ungerboeck observation model is also applied to these MIMO systems. We compared the given transmission strategies in 3-tap ISI channel with memory order J=1 and 4-tap ISI channel with memory orders J=1 and J=2 for different spectral. DDFSE provides reduction more than %75 in total computational complexity compared to the MLSE counterparts but results in higher bit error rates. Due to error propagation in DDFSE, the performance difference between spatial modulation and multiplexing is increased and spatial modulation yields an unacceptable performance in high spectral efficiencies where the multiple active spatial modulation and the BLAST structure are still satisfactory.

As future work, channel coding may be applied to the mentioned multiple antenna transmission techniques and performance of these transmission strategies with different code rates may be investigated. Also, effects of imperfect channel estimation on given multiple antenna techniques may be investigated.

REFERENCES

[1] E. Telatar, “Capacity of multi-antenna Gaussian channels,” *European Trans. Telecommun.*, vol. 10, no. 6, pp. 558–595, Nov./Dec. 1999.

[2] J. Mietzner, R. Schober, L. Lampe, W. H. Gerstacker, and P. A. Höher, “Multiple–antenna techniques for wireless communications – A comprehensive literature survey”, *IEEE Commun. Surveys Tuts.*, vol. 11, no. 2, pp. 87–105, 2nd quarter 2009.

[3] G. J. Foschini, “Layered space-time architecture for wireless communication in a fading environment when using multi-element antennas,” *Bell Syst. Tech. J.*, pp. 41–59, Autumn 1996.

[4] P. Wolniansky, G. Foschini, G. Golden, and R. Valenzuela, “V-BLAST: an Architecture for Realizing very High Data Rates over the Rich-Scattering Wireless Channel," in *URSI International Symposium on Signals, Systems, and Electronics (ISSSE '98.)*, 29 September-2 October 1998, pp. 295-300.

[5] R. Mesleh, H. Haas, C. W. Ahn, and S. Yun, “Spatial modulation–a new low complexity spectral efficiency enhancing technique,” in *Proc. Conf. Comm. and Networking in China*, Oct. 2006.

[6] R. Y. Mesleh, H. Haas, S. Sinanovic, C. W. Ahn, and S. Yun, “Spatial modulation,” *IEEE Trans. Veh. Technol.*, vol. 57, no. 4, pp. 2228–2241, July 2008.

[7] J. Jeganathan, A. Ghrayeb, and L. Szczecinski, "Spatial modulation: Optimal detection and performance analysis", *IEEE Commun. Lett.*, vol. 12, no. 8, pp. 545-547, Aug. 2008.

[8] M. Di Renzo, H. Haas, and P. M. Grant, “Spatial modulation for multiple-antenna wireless systems: a survey”, *IEEE Commun. Magazine*., vol. 49, no. 12, pp. 182−191, Dec. 2011.

[9] R.M. Legnain, R.H. M. Hafez and A. M. Legnain, “Improved Spatial Modulation for High Spectral Efficiency”, *International Journal for Distributed and Parallel Systems (IJDPS)*, vol. 3 No. 2, March 2012

[10] J. Wang, S. Jia, J. Song, “Generalised spatial modulation system with multiple active transmit antennas and low complexity detection scheme,” *IEEE Trans. Wireless Commun.*, pp. 1605-1615, Apr. 2012.

[11] Rajab M. Legnain, Roshdy H. M. Hafez, Ian Marsland and Abdelgader Legnain, "A Novel Spatial Modulation Using MIMO Spatial Multiplexing", *1st IEEE International Conference on Communications, Signal Processing, and their Applications*, Sharjah, UAE, 2013.

[12] A. Goldsmith, *Wireless Communications, Cambridge University Press,* 2005.

[13] D. Tse, and P. Viswanath, *Fundamentals of wireless communications, Cambridge University Press, Cambridge,England,* 2005.

[14] G.D. Forney. Maximum-likelihood sequence estimation of digital sequences in the presence of intersymbol interference. *IEEE Trans. Inform. Theory,* IT-18:363-378, May 1972.

[15] G. Ungerboeck, "Adaptive maximum likelihood receiver for carrier modulated data transmission systems," *IEEE Trans. Commun.*, vol. COM-22, pp. 624–635, May 1974.

[16] G. E. Bottomley and S. Chennakeshu, "Unification of MLSE receivers and extension to time-varying channels," *IEEE Trans. Commun.*, vol. 46, pp. 464–472, Apr. 1998.

[17] A. Duel-Hallen and C. Heegard, "Delayed decision-feedback sequence estimation," *IEEE Trans. Commun.*, vol. 37, pp. 428–436, May 1989.

[18] V. M. Eyuboglu and S. U. Qureshi, "Reduced-state sequence estimation with set partitioning and decision feedback," *IEEE Trans. Commun.*, pp. 13–20, Jan. 1988.

[19] A. Hafeez and W. E. Stark, "Decision feedback sequence estimation for unwhitened ISI channels with applications to multiuser detection," *IEEE J. Select. Areas Commun.*, vol. 16, pp. 1785–1795, Dec. 1998.

[20] T. S. Rappaport, *Wireless Communications: Principles and Practice, Prentice Hall,* 2nd Ed., 2002.

[21] J.G. Proakis, *Digital Communications, McGraw-Hill Science Engineering,* 3rd Ed., 1995.

[22] G. D. Forney, Jr., "The Viterbi algorithm," *Proc. IEEE,* vol. 61, pp. 268–278, Mar. 1973.

[23] M. E. Austin, "Decision-feedback equalization for digital communication over dispersive channels," M.I.T. Lincoln Lab., Lexinaton. Mass.. Tech. Reo. 437. Aug. 1967.

[24] D. G. Brennan, "Linear diversity combining techniques," *Proc. IRE,* vol. 47, pp. 1075–1102, June 1959, Reprint: *Proc. IEEE,* vol. 91, no. 2, pp. 331-356, Feb. 2003.

[25] S. M. Alamouti, “A simple transmit diversity technique for wireless communications,” *IEEE J. Select. Areas Commun.*, vol. 16, no. 8, pp. 1451–1458, Oct. 1998.

[26] Bauch, *G.*, "Space-time black codes versus space-frequency block codes", Vehicular Technology Conference, 2003. VTC 2m3-Spring. The 57th IEEE Semiannual, Vol I, pp. 567 - 571. April 2003.

[27] A. Younis, N. Serafimovski, R. Mesleh, and H. Haas, “Generalised spatial modulation,” *Proc. 2010 Asilomar Conf. on Signals, Syst. And Comput.*, pp. 1498-1502, Nov. 2010.